TVA-TR78-03

THREE-DIMENSIONAL LWR CORE SIMULATION METHODS

S. L. Forkner
G. H. Meriwether
T. D. Beu

Topical Report

Tennessee Valley Authority

June 1, 1978

TABLE OF CONTENTS

TABLE OF CONTENTS (Cont.)

LIST OF FIGURES

ABSTRACT

The CORE code was developed by TVA to simulate LWR cores over the range of conditions encountered during operation and for those analyzed during design and safety studies. The core is modeled as a three-dimensional array of rectangular nodes with coupling between neutronic and thermal-hydraulic phenomena in combination with operational parameters. The code can be used for detailed core analysis, fuel management, and optimization of operating strategies. The methods used in CORE are described in this report.

ACKNOWLEDGMENT

The following people made significant contributions to the development and implementation of the methods described in this report: T. L. Hayslett, T. F. Newton, G. W. Perry, and also H. A. Stewart who collaborated on the Appendix.

1. INTRODUCTION

Due to spatial variation of the moderator density, exposure, and fuel composition in a light water reactor (LWR), a three-dimensional steady-state reactor core simulator with thermal-hydraulic feedback is needed for core design analysis, fuel management, and optimization of operating strategies. Simulation of a large LWR requires modeling of the inter-relationships of nuclear and thermal-hydraulic phenomena in combination with operational variables. The Tennessee Valley Authority (TVA) has developed the CORE code to simulate LWR cores over the range of conditions encountered during operation and for those analyzed during design and safety studies. Due to the large number of phenomena to be represented, a compromise in the detail of some of the methods used must be made to achieve a feasible computational algorithm. The methods used in CORE are described in this report.

The reactor core is represented as a three-dimensional array of rectangular nodes, each having homogeneous internal properties. The fission source distribution is determined by a nodal coupling technique based on the TRILUX method (Reference 1-1). The neutron energy dependence can be represented by a modified one-group model or by a model which explicitly accounts for thermal neutron interchange between nodes (Reference 1-2). Nodal neutronic properties are determined by multivariable Lagrangian interpolation of input table sets of lattice physics data obtained from TVA's LATTICE code (Reference 1-3). Nodal water density, exposure, fuel temperature, control fraction, soluble boron content, and history effects are included. In addition, either transient or equilibrium xenon effects can be represented.

The thermal-hydraulic model determines the flow distribution to the individual channels and a single leakage path by equalizing the pressure drops across all flow paths. The flow quality in the channel is determined by Ahmad's method (Reference 1-4) such that both subcooled and bulk boiling are included in a consistent manner. Several void-quality relationships are available through options. The effect of direct heating of the in-channel and bypass water regions is also included. Thermal limits are determined and compared to specified values. Simulated in-core detector readings can be calculated as an option.

Depletion of the core for a cycle can be performed in a series of steps or by an optional power-exposure technique (Reference 1-5). The power-exposure algorithm calculates the Haling distribution (Reference 1-6) for use in guiding plant operations and for fuel management studies. Special fuel management options are available for the estimation of relative control rod worths, tabulation of fuel isotopic concentrations, and development of control rod patterns or fuel shuffling patterns.

The CORE code is programed in FORTRAN IV except for a few IBM 370 assembler language subroutines. Flexible dimensions allow dynamic allocation of computer storage, and a free-form input routine is used. CORE has many output edits available and extensive restart and case stacking capabilities.

CHAPTER 1 REFERENCES

1. L. Goldstein, F. Nakache, and A. Veras, "Calculation of Fuel-Cycle Burnup and Power Distribution of Dresden-1 Reactor with the TRILUX Fuel Management Program," Trans. Am. Nucl. Soc., Vol. 10, p. 300, 1967.

2. S. L. Forkner, "Two-Group Nodal Core Simulator Based on TRILUX Style Coupling," Trans. Am. Nucl. Soc., Vol. 23, p. 579, 1976.

3. B. L. Darnell, T. D. Beu, and G. W. Perry, "Methods for the Lattice Physics Analysis of LWR's," TVA-TR78-02, 1978.

4. S. Y. Ahmad, "Axial Distribution of Bulk Temperature and Void Fraction in a Heated Channel with Inlet Subcooling," J. Heat Tran., Vol. 92, pp. 595-609, 1970.

5. R. L. Crowther, "Burnup Analysis of Large Boiling-Water Reactors," Proceedings of a Panel on Fuel Burnup Predictions in Thermal Reactors, IAEA, Vienna, 1968.

6. R. K. Haling, "Operating Strategy for Maintaining an Optimum Power Distribution Throughout Life," TID-7672, 1963.

2. CORE DESCRIPTION

The reactor core is represented as a three-dimensional mesh of rectangular nodes with equal spacing in the horizontal (X,Y) direction. The axial (Z) spacing can vary from level to level if desired. The horizontal dimensions of a node normally correspond to a fuel assembly or a flow channel while the vertical dimension is specified as input. Mirror and rotational symmetry options are available for representing half or quarter core geometry. The maximum number of nodes allowed is limited only by computer resources because of the use of flexible dimensioning.

2.1 NUMBERING SYSTEM

Figure 2-1 illustrates the horizontal arrangement and numbering system for a typical (BWR) core. The minimum values of the X and Y coordinates occur at the bottom left of the figure. Both X and Y values are incremented by two at each channel location and are paired X-odd, Y-even. Locations between channels are paired X-even, Y-odd. Therefore, if control rods and in-core detectors are located between assemblies, as in a BWR, their locations are numbered with opposite parity from the channel locations. This system eliminates confusion in describing locations in the core. If control rods and in-core detectors are associated with a single channel, as in a PWR, their locations are identified by the channel X,Y coordinates. The minimum Z value is at the bottom of the core and is incremented by one for each level up the core.

The X,Y,Z coordinates are denoted by i,j,k indices for use in CORE, each of which is incremented by one for successive positions in their respective directions. The minimum i and k coordinates occur at the same positions as the minimum values of X and Z, respectively. The minimum value of j is at the same location as the maximum Y coordinate.

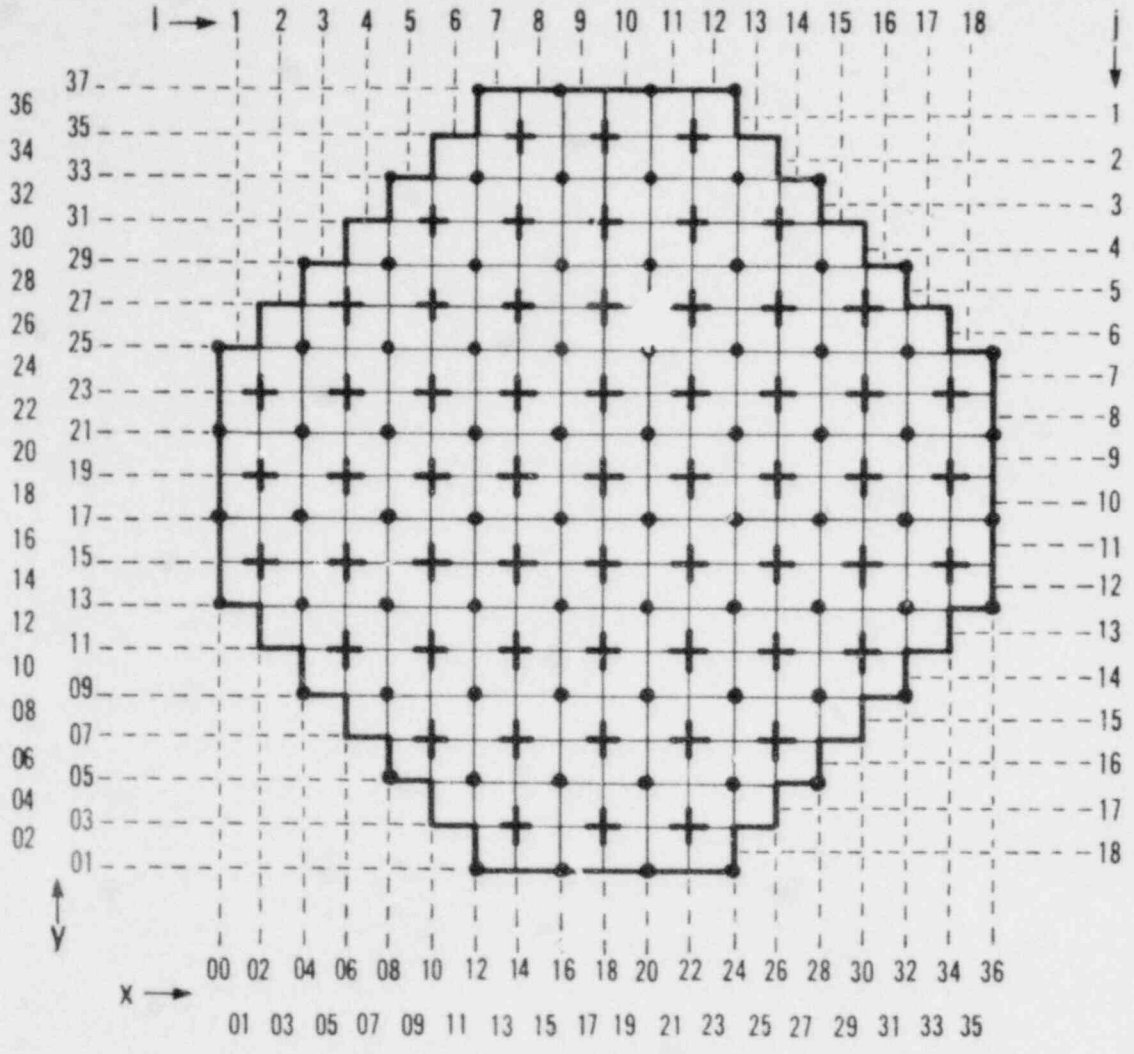

+ CONTROL ROD LOCATION

• REAL OR PSUEDO DETECTOR LOCATION

FIGURE 2-1: TYPICAL LWR PLANAR CORE MAP

2.2 PHYSICAL AND NUCLEAR FUEL TYPES

Fuel assemblies with different physical dimensions or axial variation in nuclear properties are modeled as different "physical fuel types." The physical fuel type number of each channel is defined by the input array NFT_{ij}. A zero value of NFT_{ij} indicates that the channel at location i,j lies outside the problem boundary.

The axial variation of lattice physics characteristics within physical fuel types is represented by defining "nuclear fuel types." Nuclear fuel type numbers are input in the array $NFTK_{mk}$ where the subscript m is the physical fuel type number NFT_{ij}. All channels of the same physical fuel type have the same arrangement of nuclear fuel types (Figure 2-2).

Together, the NFT_{ij} and $NFTK_{mk}$ arrays define the problem boundaries and the physical and nuclear properties of each node.

2.3 ORIFICE AND THERMAL-HYDRAULIC TYPES

Since some cores have orifices built into the core support plate to improve the flow distribution, an "orifice type" is defined for each location on the plate. Orifice type numbers are input in the NOT_{ij} array. Since the type of orifice is not dependent on the fuel assembly, the NOT_{ij} array is fixed irrespective of fuel assembly movements.

Channels with different flow and heat transfer characteristics are defined by the possible combinations of orifice and physical fuel types and are referred to as different "thermal-hydraulic types." The thermal-hydraulic type number of each channel is input in the IOT_{mn} array where the subscript m is the physical fuel type number NFT_{ij} and n is the orifice type number NOT_{ij}.

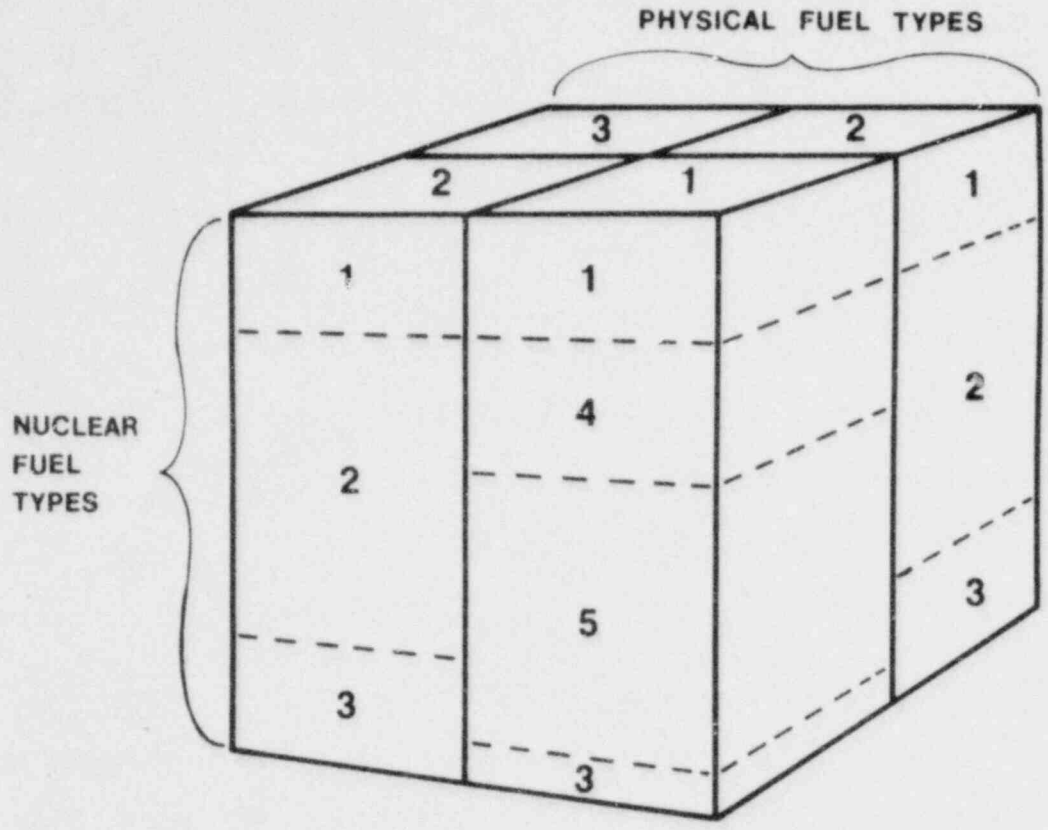

FIGURE 2-2: PHYSICAL AND NUCLEAR FUEL TYPES

3. NEUTRON TRANSPORT AND CONSERVATION MODELS

3.1 NEUTRON ENERGY DEPENDENCE

The neutronic properties of each node are determined by assuming that the node is homogeneous and by utilizing the results of a detailed lattice physics analysis for its nuclear fuel type. These analyses (Reference 3-1) account for heterogeneity effects and the spatial and energy distribution of neutrons within the node. The detailed calculations are used to determine effective homogeneous cross sections collapsed to two broad energy groups. Use of these cross sections amounts to assuming that the neutron distribution within the node is separable from the overall distribution in the reactor core. This assumption is generally good for LWR's and allows the calculations to be separated into the detailed lattice physics analyses of the nodes and the determination of the core-wide neutron balance and distribution.

In LWR's, the mean free path of thermal neutrons is small compared to the nodal dimensions. Thus, relatively few thermal neutrons escape from the node in which they are thermalized. This causes the overall distribution of neutrons in the core to be relatively insensitive to the thermal neutron tracking model. Many core simulators neglect the effects of thermal neutron interchange between nodes and use a modified one-group model in which thermal neutrons are confined to the node in which they are produced. However, CORE explicitly accounts for thermal neutron interchange using a simpler model than that used for fast neutrons. The modified one-group model is available as an option.

In cases where the assumption of homogeneous nodes may not be adequate to track thermal neutrons accurately, corrections for heterogenity

effects can be used. These corrections account for the variation in thermal neutron interchange across different faces of the node due to the location of water gaps, or a control blade for BWR's.

3.2 NEUTRON TRACKING

The overall neutron distribution in the core is calculated by considering the neutronic coupling of the nodes as treated in the TRILUX model (Reference 3-2) which can be shown to be a synthetic kernel approximation to the response matrix method (Reference 3-3). However, the implementation of the model is not identical to that in TRILUX.

3.2.1 General Neutronics Equation

The derivation of the neutronics equations (Reference 3-4) begin with the response matrix equation for an arbitrary energy group:

$$J_{ij} = P_{ij} S_i + \sum_n R_{nij} J_{ni} \qquad (3\text{-}1)$$

where

J_{ij} = the current directed from node i to node j,

S_i = the source in node i,

P_{ij} = the probability that a source neutron will escape from node i to node j,

R_{nij} = the response caused at the face of node i adjacent to node j due to neutrons impinging upon node i from node n,

and the summation is over all nodes adjacent to node i. There is a maximum of six adjacent nodes since diagonally adjacent nodes are not included.

The synthetic kernel approach allows the escape and response matrix elements to be written as a combination of simpler probabilities. One set of probabilities which can be used to approximate P_{ij} and R_{nij} is the

set of coupling coefficients defined in the development of the TRILUX equations:

σ_i = the probability that a source neutron in node i is absorbed or thermalized without escaping from node i. The probability of escaping from node i is $(1 - \sigma_i)$;

r_{ij} = the probability that a neutron escaping from node i enters the adjacent node j. Thus, the summation of r_{ij} over the six adjacent nodes is equal to one;

β_{ij} = the probability that a neutron entering node j from node i is directly absorbed in node j;

ρ_{ij} = the probability that a neutron entering node j from node i is directly reflected back to node i;

$\mu_{ij} = 1 - \beta_{ij} - \rho_{ij}$, the probability that a neutron entering node j from node i behaves like a neutron born in node j, i.e., the fraction $\mu_{ij}\sigma_j$ is absorbed without escaping node j and $\mu_{ij}(1 - \sigma_j)$ escape node j; and

$\alpha_j = \beta_{ij}/\mu_{ij}$, which depends only on properties of node j.

Using the above coupling coefficients, P_{ij} can be written as

$$P_{ij} = (1 - \sigma_i)r_{ij} \tag{3-2}$$

and the response matrix elements are

$$R_{nij} = \mu_{ni}(1 - \sigma_i)r_{ij} + \rho_{ni}\delta_{nj} \tag{3-3}$$

where δ_{nj} is the Kronecker delta which is equal to one when n = j and equal to zero otherwise. Thus, the responses at the five nonincident faces of the node are equal and the response at the incident face is larger by the direct reflection probability ρ_{ni}. Rewriting Equation (3-1) yields

$$J_{ij} = (1 - \sigma_i) r_{ij} \left[S_i + \sum_n \mu_{ni} J_{ni} \right] + \rho_{ji} J_{ji} \qquad (3\text{-}4)$$

3.2.2 Fast Neutron Tracking

Equation (3-4) is the starting point for the development of the CORE neutronics equations for the fast group. The implementation of the neutronics equations is simplified and calculational requirements are greatly reduced by elimination of the directed nodal currents J_{ij} from the neutron balance equation. The eigenfunction L_i, called the nodal leakage, is used to replace the currents and is equivalent to the total current out of node i neglecting the direct reflection terms:

$$L_i = (1 - \sigma_i) \left[S_i + \sum_n \mu_{ni} J_{ni} \right] \qquad (3\text{-}5)$$

Substituting Equation (3-5) into Equation (3-4) yields the neutron balance equation in terms of L_i:

$$L_i = \frac{\sum_j C_{ji} L_j + S_i}{\sum_j C_{ij} + A_i} \qquad (3\text{-}6)$$

where

$$C_{ij} = \frac{r_{ij}(1 - \rho_{ij})}{(1 - \rho_{ij}\rho_{ji})} \qquad (3\text{-}7)$$

$$A_i = \frac{\alpha_i + \sigma_i}{(1 + \alpha_i m_i / k_{eff})(1 - \sigma_i)} \qquad (3\text{-}8)$$

$$S_i = \frac{1}{k_{eff}} m_i A_i L_i \qquad (3\text{-}9)$$

The quantity C_{ij} is a current operator defined such that

$$J_{ij} - J_{ji} = C_{ij} L_i - C_{ji} L_j \qquad (3\text{-}10)$$

The absorption operator A_i is defined so that $A_i L_i$ represents the fast neutron absorption plus thermalization rate in the node. The parameter m_i is the nodal multiplication factor, i.e., the ratio of fast neutron production to fast absorption and thermalization. In the modified one-group model, the neutrons are assumed to be absorbed in the node in which they are thermalized, so m_i is identical to the nodal infinite multiplication factor k_∞. However, in the two-group treatment, m_i is corrected explicitly to account for net thermal neutron interchange between nodes. The eigenvalue for the problem is denoted by k_{eff}, and S_i represents the fission source of fast neutrons.

3.2.3 Thermal Neutron Tracking

Since the modified one-group model assumes no interchange of thermal neutrons between nodes, the above equations are all that are required to determine the neutron distribution in the core. However, the net exchange of thermal neutrons between nodes can have a significant effect if there is a substantial difference in the magnitude of the fast neutron source or in thermalization properties between adjacent nodes. A thermal neutron tracking model can be developed by the same method used above for the fast group (Reference 3-4).

The response matrix equation, Equation (3-1), is written for the thermal group with the fission source S_i replaced by a thermalization source Q_i:

$$Q_i = p_i A_i L_i \tag{3-11}$$

where p_i is the thermalization (or resonance escape) probability. The coupling coefficients from TRILUX are used to determine P^t_{ij} and R^t_{ij} using thermal group properties. Reference 3-4 shows that the only significant

response to a current of thermal neutrons entering a node is at the incident face, indicating that μ_{ij} for thermal neutrons can be assumed to be zero. Then the thermal current from node i to node j is given by

$$J^t_{ij} = (1 - \sigma^t_i) r_{ij} Q_i + \rho^t_{ji} J^t_{ji} \tag{3-12}$$

Using Equation (3-12) in a thermal group neutron balance with the definitions of m_i and $k_{\infty i}$ yields

$$m_i = k_{\infty i} + \frac{\overline{\eta f}_i}{A_i L_i} \sum_j \left[C^t_{ji} Q_j (1-\sigma^t_j) - C^t_{ij} Q_i (1-\sigma^t_i) \right] \tag{3-13}$$

where $\overline{\eta f}_i$ is the number of neutrons produced in fission per thermal neutron absorbed in node i, assuming that the node is homogeneous. The current operators are evaluated from Equation (3-7) using thermal group coupling coefficients. The above equation represents the effect that thermal neutron interchange between nodes has on the fast group neutronics. The thermal group neutronics is coupled to the fast group through the thermalization source Q_i.

Equation (3-13) adequately describes the effect of thermal neutron exchange between homogeneous nodes. However, the thermal current across an interface will vary depending on the orientation of the interface with respect to heterogeneities within the node. This effect is especially important in BWR's where fuel assemblies are separated by water gaps to accommodate the cruciform control blade located on two sides of each assembly. The effect of heterogeneities on the nodal multiplication factor can be accounted for by modifying the thermal current operators used in Equation (3-13).

Due to the uncertainty in evaluating the heterogeneity corrections, this effect is neglected in current practice. The modified one-group model is used for BWR's since the two-group method shows no advantage in the accuracy of results. The two-group model is normally applied to PWR's.

3.3 BOUNDARY CONDITIONS

The neutronics equation, Equation (3-6), requires coupling coefficients and the leakage L for all six nodes surrounding each node. For nodes on the problem boundary, one or more adjacent nodes will lie outside the boundary and thus are undefined. The parameters for these imaginary nodes are determined in two ways. The first of these methods is used for a symmetry boundary condition. In this case, the node outside the boundary is assumed to have the same neutronic properties and leakage as the node located symmetrically to it within the problem boundary. The second method is to apply an albedo condition at the boundary. Only albedo boundary conditions are allowed in the vertical direction, but either albedo, symmetry, or a combination of conditions can be used on the horizontal boundaries.

The albedo boundary condition is defined as

$$J_{ji} = B_i J_{ij} \tag{3-14}$$

where

J_{ji} = the current from node j outside the problem boundary to node i on the boundary,

B_i = the albedo for neutrons leaving node i toward node j, and

J_{ij} = the current from node i to node j.

Since the albedo is equivalent to the direct reflection probability of the imaginary node outside the boundary, the current operator for such nodes becomes

$$C_{ij} = \frac{r_{ij}(1-B_i)}{(1 - B_i\rho_{ij})} \qquad (3\text{-}15)$$

and Equation (3-6) can be solved for node i on the boundary. Albedos for the fast and thermal groups are input for each channel in the core. The albedo is set equal to zero for nodes which have all adjacent nodes within the problem boundary.

3.4 EVALUATION OF COUPLING COEFFICIENTS

In order to implement the neutronics models described in the previous sections, relationships must be established between the coupling coefficients and the lattice physics properties and dimensions of the node. The relationships developed here are similar to those given in Reference 3-5.

The general form of these relationships is derived from reciprocity, blackness theory, and analytic diffusion theory solutions to simple problems. In order to improve accuracy, the relationships are modified by inserting arbitrary constants at points where approximations might have affected the basic analytic equations. Values for the constants were found by minimizing the deviation of the core multiplication factor and nodal powers for a series of problems analyzed using CORE from the results obtained by fine mesh, two-group, finite-difference diffusion theory calculations. There are other procedures for determining the nodal coupling coefficients; a comparison of several different methods is presented in Reference 3-6.

3.4.1 Determination of σ

The nonleakage probability σ_i for node i is related to the blackness b_i by the approximate formula

$$b_i = \Sigma_i \bar{\ell}_i (1 - \sigma_i) \tag{3-16}$$

where

$\bar{\ell}$ = the mean chord length of the node, and

Σ = the absorption plus thermalization cross section for fast neutrons or the absorption cross section for the thermal group.

The ratio ϕ_i of the flux at the node surface to the average flux in the node is also related to blackness:

$$\phi_i = \Sigma_i \bar{\ell}_i \frac{2 - b_i}{2b_i} \tag{3-17}$$

Combining Equations (3-16) and (3-17) yields

$$\sigma_i = \frac{g_1(2\phi_i + \Sigma_i \bar{\ell}_i) - 2}{g_1(2\phi_i + \Sigma_i \bar{\ell}_i)} \tag{3-18}$$

where g_1 was introduced to account for higher order chord length terms neglected in Equation (3-16). The values of ϕ_i and g_1 are calculated from

$$\phi = 1 + \bar{\ell}\kappa \left\{ C_1 + C_2 \Delta\ell + \bar{\ell}\kappa \left[C_3 + C_4 \Delta\ell + \bar{\ell}\kappa \left(C_5 + C_6 \Delta\ell \right) \right] \right\} \tag{3-19}$$

$$g_1 = C_7 + C_8 \Delta\ell \tag{3-20}$$

where

$\kappa^2 = \Sigma/D$,

D = the diffusion coefficient,

$\Delta\ell$ = the relative difference between the nodal mean chord length and the mean chord length of a cubic node of equal volume, and

C_n = the optimized coefficients.

3.4.2 Determination of ρ and α

In order to satisfy the reciprocity theorem, the following relationship must exist between the coupling coefficients:

$$r_{ij} = \mu_{ij} F_{ij} \frac{\alpha_i + \sigma_i}{\Sigma_i \bar{\ell}_i (1-\sigma_i)} \tag{3-21}$$

The parameter F_{ij} is the fraction of the total surface area of node i shared with node j. In practice, r_{ij} is assumed equal to F_{ij} since the remaining factor is approximately equal to one.

A second relationship between the coupling coefficients is obtained by comparing the nodal neutronics equation to an analytic diffusion theory solution for a large homogeneous multiplying medium. The neutronics equation using the notation of Figure 3-1 can be written as

$$\frac{2r_X}{1+\rho_X}(L_i - L_{X+} - L_{X-}) + \frac{2r_Y}{1+\rho_Y}(L_i - L_{Y+} - L_{Y-}) +$$

$$\frac{2r_Z}{1+\rho_Z}(L_i - L_{Z+} - L_{Z-}) = \frac{(m_i^{\star} - 1)(\alpha_i + \sigma_i)}{(1+\alpha_i m_i^{\star})(1-\sigma_i)} \tag{3-22}$$

where $m_i^{\star} = m_i/k_{eff}$, the ratio of the nodal multiplication factor to the effective multiplication factor of the problem.

The asymptotic diffusion theory solution about node i in the R direction is

$$L_{R+} + L_{R-} = 2L_i \cos(B_R \Delta R) \tag{3-23}$$

where ΔR is the nodal spacing and B_R^2 is the buckling in the R direction. The cosine is approximated as a series neglecting terms higher than B_R^2 and is substituted into Equation (3-22) to obtain

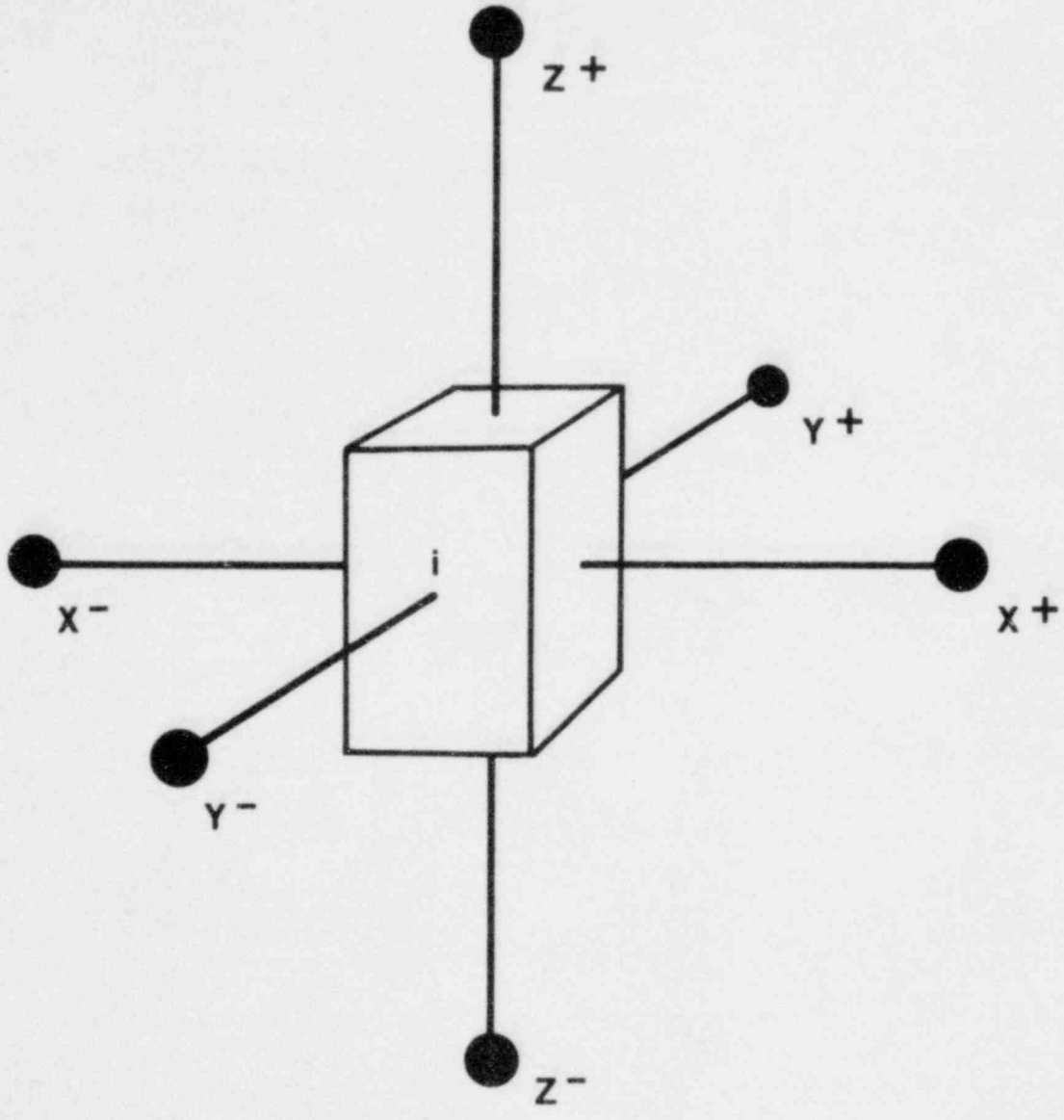

FIGURE 3-1: NOTATION FOR ADJACENT NODES IN THE NEUTRONICS EQUATIONS

$$\frac{r_X(\Delta X)^2}{1+\rho_X} + \frac{r_Y(\Delta Y)^2}{1+\rho_Y} + \frac{r_Z(\Delta Z)^2}{1+\rho_Z} = \left(\frac{\alpha+\sigma}{1+\sigma}\right)_i \left(\frac{M^2}{1+\alpha m^*}\right)_i \qquad (3\text{-}24)$$

where M^2 is the migration area of the node. The critical condition

$$\frac{m_i^*}{1+M_i^2 B_i^2} = 1 \qquad (3\text{-}25)$$

was used to eliminate the buckling from Equation (3-24).

Equations (3-21) and (3-24) are combined using the relationship

$$\begin{aligned} 1 &= \rho_{ij} + \beta_{ij} + \mu_{ij} \\ &= \rho_{ij} + \mu_{ij}(1+\alpha_i) \end{aligned} \qquad (3\text{-}26)$$

to arrive at a relationship between ρ and α:

$$\rho_{Rj} = \frac{1 - P_{Rj}\left(\frac{1+\alpha}{1+\alpha m^*}\right)_j}{1 + P_{Rj}\left(\frac{1+\alpha}{1+\alpha m^*}\right)_j} \qquad (3\text{-}27)$$

with

$$P_{Rj} = \frac{C_9 D_j}{\Delta R_j} + \frac{C_{10}}{\Sigma_j \Delta R_j} \qquad (3\text{-}28)$$

where C_9 and C_{10} are optimized coefficients. The combination of Equations (3-21) and (3-24) also gives the following quadratic equation for α:

$$a(1+\alpha)^2 + b(1+\alpha) + c = 0 \qquad (3\text{-}29)$$

where a, b, and c are dependent on P_R, m^*, σ, and nodal dimensions.

In the thermal group, the coupling coefficient μ_{ij} is zero and the parameter α_i is not used. This leads to a relationship between ρ^t and σ^t:

$$\rho_{ij}^{t} = 1 - g_2 \bar{\ell}_i \Sigma_i^{t} (1 - \sigma_i^{t}) \qquad (3\text{-}30)$$

where the superscript t denotes the thermal group. The parameter g_2 is a correction factor to account for the approximation made in Equation (3-16):

$$g_2 = C_{11} + \left(C_{12} + \frac{C_{13}}{D^{t}} \right) \Delta\ell \qquad (3\text{-}31)$$

where the C_n are optimized coefficients.

Only four of the six coupling coefficients originally defined are required to solve the neutronics equation: r_{ij}, ρ_{ij}, α_i, and σ_i. Of these, r_{ij} is approximated as being proportional to nodal dimensions. Therefore, only three coefficients are dependent on lattice physics parameters and are determined from the equations listed in the following table.

Table 3-1

Equations for Coupling Coefficients

	Fast Group	Thermal Group
σ_i	3-18	3-18
ρ_{ij}	3-27	3-30
α_i	3-28	not used

3.5 ITERATION STRATEGY

The neutronics iterations form the innermost loop of the power-leakage iteration strategy shown in Figure 3-2. The thermal-hydraulics calculations performed in the outer iteration provide the nodal operating conditions required to evaluate the lattice physics parameters at each

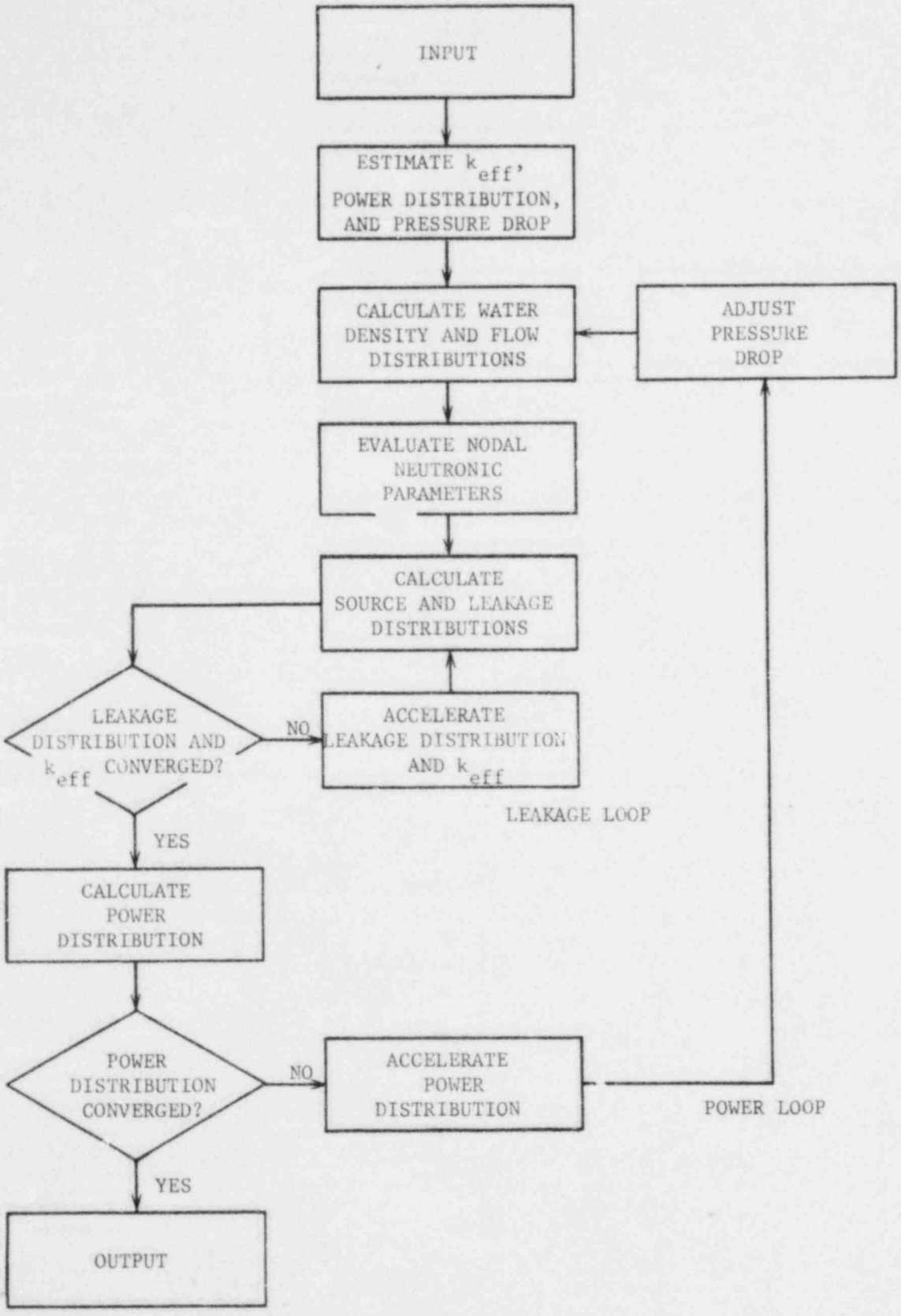

FIGURE 3-2: POWER-LEAKAGE ITERATIONS

node. Thus the nodal coupling coefficients, multiplication factor m_i, and the current and absorption operators C_{ij} and A_i in Equation (3-6) remain constant during any set of leakage iterations. However, they are updated in the outer loop due to thermal-hydraulic effects.

A successive over-relaxation procedure is used to update the leakage distribution between iterations. The sequence of calculations in the inner loop is shown below.

$$S_i^{n-1} = \frac{m_i}{k_{eff}^{n-1}} A_i L_i^{n-1} \tag{3-32}$$

$$L_i^{*} = \frac{\sum_{j=1}^{3} C_{ji} L_j^{n-1} + \sum_{j=4}^{6} C_{ji} L_j^{n} + S_i^{n-1}}{\sum_j C_{ij} + A_i} \tag{3-33}$$

$$\Delta_i^n = \frac{L_i^{*}}{\lambda^{n-1}} - L_i^{n-1} \tag{3-34}$$

$$L_i^n = L_i^{n-1} + \delta^{n-1} \Delta_i^n \tag{3-35}$$

where the superscript n is the iteration counter and δ is the over-relaxation parameter. The leakage distribution for the first set of inner iterations is estimated as either a flat or input distribution. The initial value of k_{eff} is set equal to one as is the normalization factor λ. As k_{eff} and the leakage distribution converge, the value of λ will approach unity. The normalization factor is determined for each iteration as the Rayleigh quotient of successive L_i estimates:

$$\lambda^n = \frac{\sum_i (L_i^{*})^2}{\sum_i L_i^{*} L_i^{n-1}} \tag{3-36}$$

For each iteration, the effective multiplication factor of the core is determined as follows:

$$k^{*} = \frac{\sum_{i} k_{eff}^{n-1} S_i^{n-1}}{\sum_{B} C_{ij} L_i^{n-1} + \sum_{i} A_i L_i^{n-1}} \tag{3-37}$$

$$k_{eff}^{n} = \frac{1}{2} \left(k_{eff}^{n-1} + \lambda^{n} k^{*}\right) \tag{3-38}$$

The parameter k^{*} is the multiplication factor obtained by a neutron balance using the leakage distribution from iteration n-1. The first term of the denominator of Equation (3-37) represents the leakage out of the core; thus, the summation is over only those nodal interfaces with albedo boundary conditions. Equation (3-38) is used to obtain a better estimate of the multiplication factor for each iteration; when the calculation converges, k^{*} and k_{eff}^{n} will be equal.

The leakage iterations are repeated until both k_{eff} and the leakage distribution converge within input criteria or until a specified maximum number of iterations have been performed. In a two-group calculation, the nodal multiplication factors are then recalculated from Equation (3-13). The fission power distribution is determined from the source distribution:

$$P_i = E_{Ri} S_i \tag{3-39}$$

where E_{Ri} is the energy released per fission neutron produced, obtained from the lattice physics calculations. The new P_i and two-group m_i are passed to the outer loop for the thermal-hydraulics calculations and the process repeated until the flow and power distributions and k_{eff} are converged.

CHAPTER 3 REFERENCES

1. B. L. Darnell, T. D. Beu, and G. W. Perry, "Methods for the Lattice Physics Analysis of LWR's," TVA-TR78-02, 1978.

2. L. Goldstein, F. Nakache, and A. Veras, "Calculation of Fuel-Cycle Burnup and Power Distribution of Dresden-1 Reactor with the TRILUX Fuel Management Program," Trans. Am. Nucl. Soc., Vol. 10, p. 300, 1967.

3. Z. Weiss, "Some Basic Properties of the Response Matrix Equations," Nucl. Sci. & Eng., Vol. 63, pp. 457-492, 1977.

4. S. L. Forkner, "Two-Group Nodal Core Simulator Based on TRILUX Style Coupling," Trans. Am. Nucl. Soc., Vol. 23, p. 579, 1976.

5. Z. Weiss, "Nodal Equations Derived from Invariant Imbedding Theory," Nucl. Sci. & Eng., Vol. 48, pp. 233-247, 1972.

6. A. Ancona, et al , "Nodal Coupling by Response Matrix Principles," Nucl. Sci. & Eng., Vol. 64, pp. 405-417, 1977.

4. THERMAL-HYDRAULIC MODELS

Because of the dependence of the nodal lattice physics data on nodal operating parameters, the thermal-hydraulic model of the core has a significant effect on the calculation of the reactivity and power distribution. Another important neutronic coupling to the thermal-hydraulic calculation is through the Doppler effect on reactivity with its dependence on fuel temperature. Thus, the thermal-hydraulic analysis may be considered of equal importance as the neutronics analysis in a core simulator.

Formulas from the 1967 ASME Steam Tables (Reference 4-1) are used to evaluate the required water and steam properties as a function of system pressure and inlet enthalpy.

4.1 FLOW DISTRIBUTION

For a specified total core flow rate, the flow rate through each channel and a single leakage path is determined by equalizing the pressure drops across all flow paths. The pressure drop is determined by contributions from elevation, friction, acceleration, and local losses which are influenced by the channel thermal-hydraulic type, coolant density, and crud thickness. The flow through the channel is also a function of the total channel power, the axial power shape, the inlet subcooling, and the reactor pressure.

To avoid performing repetitive calculations of pressure drop and flow for the large number of channels in a LWR core, the detailed thermal-hydraulic calculations are performed externally to the CORE code. The THAS single-channel code developed by TVA does the thermal-hydraulic calculations for each channel thermal-hydraulic type using a specified

symmetric axial power distribution, inlet subcooling and reactor pressure. These calculations are repeated for several channel powers at varying flow rates to determine the pressure drop. The results are combined into two-dimensional tables of flow rate versus channel power and pressure drop for use in CORE. The methods used in THAS are described in the Appendix.

The flow in individual channels is determined by Lagrangian interpolation in the base table for the channel thermal-hydraulic type. The base channel flow W_o is then corrected for increased flow resistance due to crud buildup, and for variations of the reactor pressure, inlet subcooling, and axial power shape from the assumed table values. THAS calculations are made to determine the effect that varying the above parameters has on the flow rate. The actual channel flow W_c is least squares fit using the THAS results to a quadratic equation for use in the code:

$$aW_c^2 + bW_c + c = 0 \tag{4-1}$$

The coefficients in Equation (4-1) are

$$a = \frac{C_0 + f\left[C_1 + \chi_{in}(C_2 + \chi_{in}C_3)\right]}{\rho_{in}} \tag{4-2}$$

$$b = \frac{1}{\rho_{in}}\left[(C_4 + C_5\ fV)\ \frac{P_c}{H_{fg}} + C_6\ \chi_{in}\ \frac{H_{fg}}{P_c}\right] \tag{4-3}$$

$$c = \rho_{in} - \rho_{in}^o - W_o(b_o + a_o W_o) \tag{4-4}$$

where the o denotes quantities evaluated at base conditions,

f = a crud thickness factor,

χ_{in} = the inlet quality,

ρ_{in} = the inlet density,

H_{fg} = the heat of vaporization,

P_c = the channel power,

C_n = the fitting constants, and

V = a channel power shape parameter

$$= \frac{\sum_{k=1}^{K} P_k \, \Delta Z_k \left(1 - \frac{Z_k}{L}\right)}{\sum_{k=1}^{K} P_k \, \Delta Z_k} \qquad (4\text{-}5)$$

with P_k = the relative power in node k,

ΔZ_k = the length of the node,

Z_k = the distance from the bottom of the active core to the center of node k,

L = the total length of the fuel rods, and

K = the number of axial levels in the core.

The core leakage flow is computed by setting the pressure drop in the bypass region equal to the sum of the elevation head and bypass region entrance losses. For the purpose of calculating the leakage flow rate, it is assumed that the coolant mixes uniformly in the bypass region; thus, all bypass regions are lumped together.

In determining the channel and leakage flow rates, the value of the core pressure drop is assumed to be known. Normally, the pressure drop is not known a priori and must be considered as a function of the flow rate as well as the parameters affecting the flow rate. The pressure drop is usually estimated initially and adjusted between thermal-hydraulic iterations by forcing the sum of the calculated channel and leakage flow rates to equal the specified value of the total core flow.

4.2 HEAT SOURCE DISTRIBUTION

The heat addition to the coolant flowing through the core is the sum of three components. Most of the heat deposited in the coolant is transferred from the fuel through the clad. Smaller fractions are added directly to in-channel and bypass water by neutron thermalization or gamma heating in the coolant or in structural material in the channel and then transferred to the coolant. The heat flux distribution is proportional to the fission power distribution calculated by the neutronics model. The direct heating components are determined by the energy deposition distribution for fast neutrons and gamma rays which tends to be smoother than the fission power distribution. The distribution of fast neutrons and gammas in the core is estimated by

$$\psi_{ijk} = \gamma + (1-\gamma)P_{ijk} \qquad (4\text{-}6)$$

where γ is an input parameter which is equal to one for a uniform distribution and zero for a distribution identical to the relative fission power distribution P_{ijk}.

4.2.1 In-channel Distribution

The contribution of direct heating of in-channel water to the total core heat rate is

$$Q^{d}_{ijk} = C\ F_d\ \bar{P}_n\ \psi_{ijk}\ d_{ijk} \qquad (4\text{-}7)$$

where

F_d = the fraction of core power from direct heating of in-channel water,

$\bar{P}_n$ = the average nodal power in the core,

d_{ijk} = the direct heating energy deposition distribution, which is proportional to the local water density, and

C = a proportionality constant.

Thus, the in-channel heat addition distribution is the sum of its components:

$$Q^c_{ijk} = q''_{ijk} S_{ijk} + Q^d_{ijk} \quad (4\text{-}8)$$

where q''_{ijk} is the heat flux out of the clad, and S_{ijk} is the surface area of the clad in the node.

4.2.2 Bypass Region Distribution

The contribution to the core heat rate from direct heating of the bypass region water is

$$Q^b_{ijk} = C F_b \bar{P}_n \psi_{ijk} \quad (4\text{-}9)$$

where F_b is the fraction of power from direct heating of the bypass region water, and depends on whether the adjacent nodes are controlled or uncontroiled. Since the variation of water density in the bypass region is small, its effect on the energy deposition distribution is neglected, and d_{ijk} is set equal to one. In addition, the fission power P_{ijk} used in Equation (4-6) to evaluate ψ_{ijk} in the bypass region must be a weighted average of the fission powers of the nodes surrounding the bypass region between fuel assemblies.

4.3 COOLANT CONDITIONS

The neutronics calculations are coupled to the thermal-hydraulic analysis through the dependence of lattice physics parameters on local operating conditions. Especially important is the effect water density

has on reactivity and the power distribution. The bulk coolant temperature in the channel is also required to calculate the effective fuel temperature (Section 4.4) for the evaluation of the Doppler effect on reactivity.

In normal operation of a LWR, subcooled coolant enters at the bottom of the core and is heated as it moves up the channel. This can lead to a maximum of four flow regimes with characteristic coolant conditions:

a) the nonboiling regime where the coolant remains subcooled,
b) the wall voidage regime where steam bubbles form but do not detach from the fuel rod surface,
c) the subcooled boiling regime where the steam bubbles detach and may recondense in the subcooled liquid phase, and
d) the bulk boiling regime where the liquid is at the saturation temperature and the steam bubbles are not recondensed.

The following sections present the methods used to calculate the bulk coolant temperature and density in each flow regime. The effect of steam formation in the bypass region between fuel assemblies in BWR's is also discussed.

4.3.1 Nonboiling Regime

In this flow regime, the coolant is subcooled and the surface temperature of the fuel rods is below the saturation temperature. No vapor is formed and thermal equilibrium exists. Thus, the average bulk coolant temperature in the node is calculated by an energy balance:

$$T_b = T_i + \frac{Q_c}{GA_f C_p} \qquad (4\text{-}10)$$

where

T_i = the average bulk coolant temperature in the previous node,

Q_c = the heat addition to the in-channel coolant between the midpoints of the nodes,

G = the mass flux through the node,

A_f = the flow area of the node, and

C_p = the specific heat of the coolant.

The coolant density is calculated from the 1967 ASME formulas as a function of bulk coolant temperature and system pressure.

4.3.2 Wall Voidage Regime

In the wall voidage regime, steam bubbles are formed on the heating surface, but do not detach from the wall. Heat transfer from the wall is enhanced by agitation of the coolant layer adjacent to the wall caused by the growth and subsequent collapse of bubbles on the surface. There is a negligible net generation of vapor; thus, all the heat goes to raise the bulk liquid temperature and thermal equilibrium can be assumed.

The bulk coolant temperature is calculated from Equation (4-10) as for the nonboiling flow region. The coolant density is computed from the equation

$$U = \rho_f - \alpha(\rho_f - \rho_g) \qquad (4\text{-}11)$$

where

ρ_f = the density of saturated water,

ρ_g = the density of saturated steam, and

α = the void fraction in the node.

The void fraction is calculated from Griffith's model discussed in Reference 4-2:

$$\alpha = \delta \frac{P_h}{A_f} \tag{4-12}$$

where P_h is the heated perimeter and δ is the bubble layer thickness given by

$$\delta = \frac{\left[q'' - h(T_w - T_b)\right] Pr_b k_b}{1.07h^2 (T_s - T_b)} \tag{4-13}$$

The single phase heat transfer coefficient is

$$h = 0.030 \frac{k_b}{D_e} Re_b^{0.8} Pr_b^{0.4} \tag{4-14}$$

and the wall temperature is calculated from the Jens and Lottes equation:

$$T_w = T_s + \frac{60 (q'' x 10^{-6})^{1/4}}{e^{P/900}} \tag{4-15}$$

Other parameters appearing in Equations (4-13), (4-14), and (4-15) are

a) the surface heat flux q",

b) the bulk coolant thermal conductivity k_b,

c) the bulk coolant Prandtl and Reynolds numbers Pr_b and Re_b,

d) the saturation temperature T_s,

e) the equivalent diameter of the channel D_e, and

f) the reactor pressure P.

4.3.3 Subcooled Boiling Regime

The subcooled boiling regime is defined as that between the onset of bubble detachment and the beginning of bulk boiling. Vapor bubbles detach from the heating surface and can eventually recondense in-stream in the subcooled liquid. Thus, heat transfer is enhanced due to the mixing of the steam bubbles in the subcooled liquid before collapse. Since vapor and subcooled liquid exist simultaneously, the assumption of thermal equilibrium

is not applicable and the calculation of coolant conditions becomes complex. However, the bulk temperature and density can be determined if the quality is known and a slip model for the liquid and vapor phases is specified. A modified version of Ahmad's method (Reference 4-3) is used to calculate coolant conditions in the subcooled boiling regime.

In subcooled boiling, the total heat flux is divided into two components

$$q'' = q''_{\ell} + q''_{\lambda} \tag{4-16}$$

where q''_{ℓ} is the portion that raises the temperature of the liquid phase and q''_{λ} is the part which produces boiling. Ahmad assumed that

$$q''_{\ell} = h_{\ell}\Delta T \tag{4-17}$$

where $\Delta T = T_s - T_b$ is the local subcooling, and developed a correlation for the subcooled boiling liquid phase heat transfer coefficient:

$$h_{\ell} = 2.44 \frac{k_b}{D_e} Re_b^{1/2} Pr_b^{1/3} \left(\frac{H_{in}}{H_f}\right)^{1/3} \left(\frac{H_{fg}}{H_f}\right)^{1/3} \tag{4-18}$$

where H_{in} is the inlet enthalpy and H_f is the enthalpy of the saturated liquid. The axial level in the channel where bubble detachment occurs can be determined by finding the point Z_d where the subcooling calculated using Equation (4-10) is less than the subcooling required for detachment ΔT_d obtained from Equation (4-17). Cases where ΔT_d exceeds the inlet subcooling ΔT_{in} signify that subcooled boiling occurs from the start of the heated length, and ΔT_d is set equal to ΔT_{in} with Z_d set equal to zero.

Ahmad wrote an energy balance on a length of heated channel in subcooled boiling using several simplifying assumptions to obtain a differential equation for the bulk coolant temperature in dimensionless form:

$$\frac{d(\Delta T^*)}{dZ^*} = -\left(C_1 + \frac{3}{2} C_2 \sqrt{Z^*}\right) \Delta T^* \qquad (4\text{-}19)$$

The dimensionless subcooling ΔT^* is the ratio of the local subcooling to the subcooling at bubble detachment. The dimensionless distance Z^* is

$$Z^* = \frac{Z - Z_d}{Z_{sb}} \qquad (4\text{-}20)$$

where Z is the axial distance up the core and Z_{sb} is the total significant boiling length up the channel from Z_d. The heat transfer parameter C_1 and the condensation parameter C_2 are

$$C_1 = \frac{h_\ell P_h Z_{sb}}{G A_f C_p} \qquad (4\text{-}21)$$

$$C_2 = \frac{2}{3} \frac{K H_{fg} Z_{sb}^{3/2}}{G A_f C_p} \qquad (4\text{-}22)$$

where K is a condensation constant proportional to the square of the heat flux. For practical problems, the condensation of steam bubbles in subcooled boiling is very slow due to the high flow rate through the channel; thus, the condensation parameter C_2 is usually very small and the second term in Equation (4-19) can normally be neglected.

Assuming a uniform heat flux, Equation (4-19) can be solved to give

$$\Delta T^* = \exp\left[-\left(C_1 Z^* + C_2 Z^{*\,3/2}\right)\right] \qquad (4\text{-}23)$$

The heat flux in a LWR normally will not be uniform over the entire channel, but the assumption of a uniform heat flux inside each node allows the heat flux to vary axially in steps and is consistent with the neutronics model.

Thus, the bulk coolant temperature in each node can be determined from Equation (4-23) using the outlet conditions of the lower node to evaluate the required parameters:

$$T_b = T_s - \Delta T_d \, \Delta T^* \tag{4-24}$$

The average coolant density in subcooled boiling is found using Equation (4-11) with the void fraction

$$\alpha = \frac{\chi}{\chi + \frac{\rho_g}{\rho_f} S(1-\chi)} \tag{4-25}$$

where S is the slip ratio determined below. The flow quality obtained from Ahmad's method is

$$\chi = \frac{AZ^* - 1 + \Delta T^*}{B + \Delta T^*} \tag{4-26}$$

where

$$A = \frac{Q_c}{GA_f C_p \Delta T_d} \tag{4-27}$$

$$B = \frac{H_{fg}}{C_p \Delta T_d} \tag{4-28}$$

The quantity Q_c in Equation (4-27) is the total heat addition to the in-channel coolant, including the direct heating contributions, between Z_d and the position of interest, and can be calculated using Equation (4-8). Thus, the effect of nonuniform heat flux is also included in the calculation of quality. It should be noted that the Levy equation used in THAS for flow quality (Reference 4-4) is an approximation to Equation (4-26) for the special case where $\Delta T_d < \Delta T_{in}$ and in-stream bubble condensation is negligible ($C_2 = 0$).

Development of a general model for the slip ratio is difficult due to its dependence on the flow, the physical properties of the coolant, and the channel geometry. Most slip models are based upon empirical correlations of data taken under a limited range of conditions. Several slip models are available as options, but the CISE model (Reference 4-5) is normally used. The CISE slip ratio is obtained as follows:

$$Y = \frac{\alpha_h}{1-\alpha_h} \tag{4-29}$$

$$T = \frac{Y}{1+C_3 Y} - C_3 Y \tag{4-30}$$

$$S = \begin{cases} 1.0 & T \leq 0 \\ 1.0 + C_4\sqrt{T} & T > 0 \end{cases} \tag{4-31}$$

where α_h is the void fraction assuming homogeneous flow [S = 1 in Equation (4-25)] and the C's are empirical parameters

$$C_3 = 0.0273\ Re^{-0.51}\ Wb \left(\frac{\rho_f}{\rho_g}\right)^{-0.08} \tag{4-32}$$

$$C_4 = 1.578\ Re^{-0.19} \left(\frac{\rho_f}{\rho_g}\right)^{0.22} \tag{4-33}$$

where Wb is the Weber number.

4.3.4 Bulk Boiling Regime

The bulk boiling flow regime begins where the bulk coolant reaches the saturation temperature. The total heat addition is utilized in the production of vapor; thus, the bulk coolant temperature remains constant at the saturation temperature. The average in-channel coolant density is determined using the same method as for the subcooled boiling regime.

4.3.5 Bypass Region Effects

The bypass water between fuel assemblies in a BWR can experience boiling which may significantly affect the lattice physics properties of the adjacent nodes through a reduction in moderator density. This effect is accounted for by using an effective nodal water density in the neutronics calculations:

$$U_{eff} = U + \alpha_{bp}(\rho_f - \rho_g)\left(C_1 + \frac{C_2}{U}\right) \tag{4-34}$$

where U is the in-channel water density, α_{bp} is the void fraction in the bypass region associated with the node, and the C's are fitting constants which depend on the channel thermal-hydraulic type. Data for the fits is obtained from detailed lattice physics calculations by varying in-channel and bypass water densities.

The void fraction in the bypass region is calculated using Equation (4-25) with the CISE slip model. The required bypass quality is determined from an energy balance assuming thermal equilibrium between the liquid and vapor phases:

$$X_{bp} = \frac{\frac{Q_b}{W_{bp}} + H_{in} - H_f}{H_{fg}} \tag{4-35}$$

where Q_b is the total heat addition rate to the bypass water up to the midpoint of the node. The flow rate W_{bp} in the bypass region surrounding each channel is assumed to be the same and thus can be calculated by dividing the total leakage flow by the number of channels in the core. Since the rate of heat addition in the bypass region is low, the assumption of thermal equilibrium does not lead to significant error.

4.4 EFFECTIVE FUEL TEMPERATURE

The neutronic and thermal-hydraulic analyses are coupled through the dependence of the Doppler reactivity effect on fuel temperature. Since the Doppler correction is applied on a nodal basis, a method of calculating the effective fuel temperature in each node is required.

By using a detailed fuel rod thermal-mechanical code, the temperature distribution in individual pin segments can be determined as a function of power and exposure for each fuel design. The effective fuel temperature for pin i is calculated as a weighted average of the volume averaged and surface temperatures of the fuel:

$$T_f^i = \alpha T_{avg}^i + (1-\alpha) T_{sur}^i \qquad (4\text{-}36)$$

where α is the weighting factor, typically about 0.85 (Reference 4-6).

To arrive at the proper value of the nodal effective fuel temperature, the variation of power and exposure from pin to pin within the node must be taken into account. The individual pin powers and exposures can be determined from the nodal average values with the aid of the pin-by-pin relative power distribution calculated by TVA's LATTICE physics code (Reference 4-7). Since exposure is directly proportional to the time integral of power, the pin-by-pin relative exposure distribution in the node can be obtained by integrating the power distributions from a series of LATTICE calculations at different nodal average exposures. Thus, the pin powers and exposures can be calculated by multiplying the nodal average value by the appropriate distribution. The individual pin effective fuel temperatures are calculated from Equation (4-36) and averaged to obtain the nodal value of the fuel temperature.

The results of the above calculations are reduced to the following equation for use in the core simulator:

$$T_f = T_b + \bar{q}' \left\{ C_1 + E(C_2 + C_3 E) + \bar{q}' [C_4 + E(C_5 + C_6 E)] \right\} \qquad (4\text{-}37)$$

where

T_b = the bulk coolant temperature in the node,

$\bar{q}'$ = the nodal average linear heat generation rate,

E = the nodal average exposure, and

C_n = fitting coefficients.

CHAPTER 4 REFERENCES

1. C. A. Meyer, et al., "Thermodynamic and Transport Properties of Steam," American Society of Mecnanical Engineers, 1967.

2. G. W. Maurer, "A Method of Predicting Steady-State Boiling Vapor Fractions in Reactor Coolant Channels," WAPD-BT-18, 1960.

3. S. Y. Ahmad, "Axial Distribution of Bulk Temperature and Void Fraction in a Heated Channel With Inlet Subcooling," J. Heat Tran., Vol. 92, pp. 595-609, 1970.

4. S. Levy, "Forced Convection Subcooled Boiling - Prediction of Vapor Volumetric Fraction," GEAP-5157, 1966.

5. A. Premoli, et al., "An Empirical Correlation for Evaluating Two-Phase Mixture Density Under Adiabatic Conditions," An Informal Contribution to the Private Meeting, Heat Transfer Laboratory, Grenoble, France, 1970.

6. D. H. Risher, Jr., "An Evaluation of the Rod Ejection Accident in W PWR's Using Spatial Kinetics Methods," WCAP-7588, 1975.

7. B. L. Darnell, T. D. Beu, and G. W. Perry, "Methods for the Lattice Physics Analysis of LWR's," TVA-TR78-02, 1978.

5. LATTICE PHYSICS DATA REPRESENTATION

The neutronics and thermal-hydraulic analyses are coupled through the dependence of the lattice physics parameters on the operating conditions at each node. The lattice physics data required for the neutronics calculations is obtained from detailed analyses of each nuclear fuel type represented by a single fuel assembly and its surrounding water (Reference 5-1). These analyses are performed parametrically as a function of in-channel water density, assembly average exposure, and exposure-history dependent in-channel water density, with the control rod either withdrawn or inserted during the analysis. The spatially averaged two-group lattice physics parameters are represented by polynomial fits and by Lagrangian interpolation of tabulated values for each nuclear fuel type.

5.1 LATTICE PHYSICS TABLE SETS

Most of the lattice physics parameters are functions of the in-channel water density U, exposure E, and the control fraction CF (the fraction of the node height a control rod is inserted). Since the dependence on these variables tends to be nonseparable, the basic method for representing lattice physics data is in sets of tables at specific values of U, E, and CF. Multi-variable Lagrangian interpolation is used to obtain nodal parameters at the required values of U, E, and CF. The following parameters are represented by the U-E-CF table sets:

a) the infinite multiplication factor k_∞,

b) the fast fission factor ε,

c) the thermalization or resonance escape probability p,

d) the age-to-thermal τ,

e) the fast absorption plus removal cross section Σ_o,

f) the thermal absorption cross section Σ_a,

g) the thermal diffusion area L^2,

h) the xenon thermal microscopic absorption cross section σ_X,

i) the xenon reactivity worth ρ_X,

j) the reactivity worth ρ_C of depletion with the control rod inserted versus depletion with the rod withdrawn,

k) the energy release per fission neutron produced E_R,

l) the fissile and fertile fuel isotopic concentrations, and

m) the reactivity effect of water density history UH for BWR's or the soluble boron concentration PPM for PWR's.

Due to variation in operating parameters, the in-channel water density will not be constant nor can control rod positions be maintained throughout the cycle. These effects are accounted for by defining exposure history dependent variables. The water density history is defined as

$$UH(E) = E\ \bar{U}(E) \tag{5-1}$$

where $\bar{U}$ is the exposure averaged in-channel water density

$$\bar{U}(E) = \frac{1}{E}\int_0^E U(E)dE \tag{5-2}$$

The control history CH is defined similarly using the exposure averaged control fraction $\overline{CF}$.

For lattice physics parameters a-k above, the table sets assume that the node was depleted at the instantaneous in-channel water density

with the control rod withdrawn throughout the depletion, i.e., $\bar{U} = U$ and $\overline{CF} = 0$. Depletion at a constant soluble boron concentration PPM_o is also assumed for PWR's. Corrections made for deviation of $\bar{U}$, $\overline{CF}$, and PPM from the base values are discussed in Section 5.2. Since the nodal multiplication factor for BWR's is very sensitive to the water density history, the correction to k_∞ due to deviation of $\bar{U}$ from U is included in the lattice physics tables for greater accuracy (item m). For PWR's, the correction to k_∞ due to variation of PPM from PPM_o is tabulated as item m for the same reason. Fuel isotopic concentrations (item 1) are related to history dependent rather than instantaneous values of water density and control fraction. Thus, the isotopics are interpolated from the tables as a function of exposure using $\bar{U}$ and $\overline{CF}$ instead of U and CF.

5.2 CORRECTIONS TO NODAL LATTICE PHYSICS PARAMETERS

The lattice physics table sets assume base values or fixed relationships for nodal independent variables that are not as closely coupled as are U, E, and CF. These variables include the fuel temperature, the moderator temperature, the equilibrium xenon concentration corresponding to the base power density, and the soluble boron concentration. Many of the lattice physics parameters are not sensitive to deviation of such variables from th assumed base values. In these cases, the parameter is determined solely by interpolation in the table sets. Other parameters, most notably the nodal multiplication factor k_∞, must be evaluated by correction of the interpolated values to account for the variation of independent variables from values assumed in the tables.

5.2.1 Doppler Effect

Deviation of the nodal fuel temperature T_f from the base value T_f^o affects the nodal multiplication factor k_∞ through Doppler broadening

of resonances in the fuel. This effect is accounted for by a correction to the base k_∞ from the lattice physics tables:

$$C_D = \alpha_D\left(\sqrt{T_f} - \sqrt{T_f^o}\right) \tag{5-3}$$

where the Doppler coefficient α_D is fit to a function dependent on U and E.

In addition to correcting k_∞, C_D is also used to make corrections to other parameters affected by changes in resonance absorption, including the age-to-thermal, the absorption plus removal cross section, and the thermalization probability. The correction factor for Σ_o and p is simply the ratio of the Doppler corrected k_∞ to the base k_∞; the correction factor for τ is the inverse ratio.

5.2.2 Moderator Temperature

The lattice physics tables assume a fixed relationship between the moderator temperature and the in-channel water density at a base reactor pressure. Subcooled boiling or variations from the nominal reactor pressure can cause the nodal moderator temperature calculated in the thermal-hydraulic analysis to differ from the base temperature. The correction to the base k_∞ due to this effect is the factor:

$$C_M = 1 + f_M(T_m - T_m^o) \tag{5-4}$$

where

T_m = the nodal moderator temperature,

T_m^o = the base moderator temperature, and

f_M = a fitting function which is dependent on U, E, CF, T_m, and the soluble boron concentration.

5.2.3 Water Density History

The lattice physics tables for items a-k assume that the exposure averaged and instantaneous water densities are equal. This assumption may be inadequate for PWR's where the nodal in-channel water density can vary greatly depending on operating conditions. Thus, for BWR's the effect of water density history on the nodal k_∞ is accounted for by multiplying the base k_∞ by a correction factor obtained by interpolation in lattice physics tables (item m). These tables contain the ratio of k_∞ at a specified $\bar{U}$ to the base k_∞ for three values of $\bar{U}$. Quadratic interpolation between the three values determines the water density history effect for any nodal value of $\bar{U}$.

Since PWR's do not experience as large a variation in water density, the correction factor for the nodal k_∞ is expressed as a polynomial fit:

$$C_{UH} = 1 + E(U-\bar{U}) \left[f_{UH1}(1-CF) + f_{UH2}\ CF \right] \qquad (5\text{-}5)$$

The fitting functions f_{UH1} and f_{UH2} are dependent on E and $(U-\bar{U})$.

5.2.4 Control History

The lattice physics table sets assume that the node is depleted with the control rod always fully withdrawn from the node. To account for the effect of previous control rod insertions, the nodal multiplication factor is multiplied by a factor dependent on the exposure averaged control fraction:

$$C_C = 1 + \rho_C\ \overline{CF} \qquad (5\text{-}6)$$

where ρ_C is the reactivity worth if depleted in a fully controlled condition ($\overline{CF} = 1$) as opposed to the base case of $\overline{CF} = 0$, and is determined by interpolation in a table set (item j).

5.2.5 Xenon Concentration

The poisoning effect of the highly absorbing fission product Xe-135 must be included in determining the nodal k_∞. The base k_∞ interpolated from the tables (item a) incorporates the effect of the equilibrium xenon concentration at the base power density assumed in the table. The effect of the actual nodal xenon concentration on k_∞ is accounted for by a correction factor related to the fractional variation from the base concentration:

$$C_X = 1 - f_X \rho_{X_o} \left(\frac{X - X_o}{X_o} \right) \qquad (5\text{-}7)$$

where

X = the nodal xenon concentration,

X_o = the equilibrium xenon concentration corresponding to the base power density,

ρ_{X_o} = the reactivity worth of the base xenon concentration, interpolated from the tables (item i), and

f_X = a fitting function that corrects ρ_{X_o} for deviation of the soluble boron concentration from the base value.

The actual xenon concentration can be input from a previous case or set equal to zero, or can be calculated as the equilibrium value for the actual power density in the node or from the transient iodine and xenon equations.

5.2.6 Soluble Boron Concentration

The lattice physics table sets for items a-k for PWR's assume a soluble boron concentration PPM equal to the base value PPM_o. Since the nodal k_∞ is sensitive to the soluble boron concentration, a

correction factor to account for variations of PPM from PPM_o is interpolated from the table set for item m for PWR's as was done for the water density history effect for BWR's. Soluble boron is not used in BWR's except in an auxiliary shutdown system; thus the dependence of BWR nodal k_∞ on PPM is expressed as a polynomial correction factor to the base k_∞:

$$C_{PPM} = 1 + f_{PPM} (PPM - PPM_o) \tag{5-8}$$

The fitting function f_{PPM} depends on U, E, CF, PPM, and the relative xenon concentration.

Since the soluble boron affects the spectrum in the node, the cross sections are also affected by a deviation of PPM from PPM_o. The xenon cross section is modified as follows to account for the spectral shift:

$$\sigma_X = \sigma_X^o [1 + KU(PPM - PPM_o)] \tag{5-9}$$

where K is a fitting constant. The effect on other cross sections is lumped into a correction to the nodal macroscopic thermal absorption cross section described in the following subsection.

5.2.7 Combination of Correction Factors

The nodal multiplication factor k_∞ is calculated from the base value k_∞^o by combining the correction factors discussed in the previous subsections:

$$k_\infty = k_\infty^o (1 + C_D) C_M C_{UH} C_C C_X C_{PPM} \tag{5-10}$$

Since both xenon and soluble boron compete with other materials in the node for thermal neutrons, the thermal group constants Σ_a and L^2 must be corrected for deviation of xenon and soluble boron concentrations from

the base values. The correction factors for these two parameters are proportional to the relative change in k_{∞} caused by the variation of both xenon and soluble boron.

CHAPTER 5 REFERENCE

1. B. L. Darrell, T. D. Beu, and G. W. Perry, "Methods for the Lattice Physics Analysis of LWR's," TVA-TR78-02, 1978.

6. REACTIVITY DEPLETION

6.1 FORWARD STEP METHOD

The forward step method is used to simulate depletion with core operating conditions that change during the cycle. The core average exposure is incremented in steps during which the operating parameters (control rod pattern, core power, flow rate, etc.) experience only minor variations. Figure 6-1 diagrams the sequence of calculations for the forward step method of depletion.

Using representative operating parameters for the step and the nodal fuel properties (exposure E, water density history UH and control history CH) calculated at the end of the previous step, the core multiplication factor k_{eff} and relative power distribution P are determined by the power-leakage iterations. A restart file containing the power distribution, nodal fuel properties and other information is output for use in later cases. The fuel properties can be updated for the next step:

$$E_{ijk}^{n+1} = E_{ijk}^{n} + P_{ijk}^{n} \Delta E^{n} \frac{\overline{WT}}{WT_{ijk}} \tag{6-1}$$

$$UH_{ijk}^{n+1} = UH_{ijk}^{n} + U_{ijk}^{n} P_{ijk}^{n} \Delta E^{n} \frac{\overline{WT}}{WT_{ijk}} \tag{6-2}$$

$$CH_{ijk}^{n+1} = CH_{ijk}^{n} + CF_{ijk}^{n} P_{ijk}^{n} \Delta E^{n} \frac{\overline{WT}}{WT_{ijk}} \tag{6-3}$$

where

U_{ijk} = the effective nodal water density,

CF_{ijk} = the control fraction of the node,

WT_{ijk} = the mass of heavy metal per unit length in the node, and

$\overline{WT}$ = the core average mass of heavy metal per unit length.

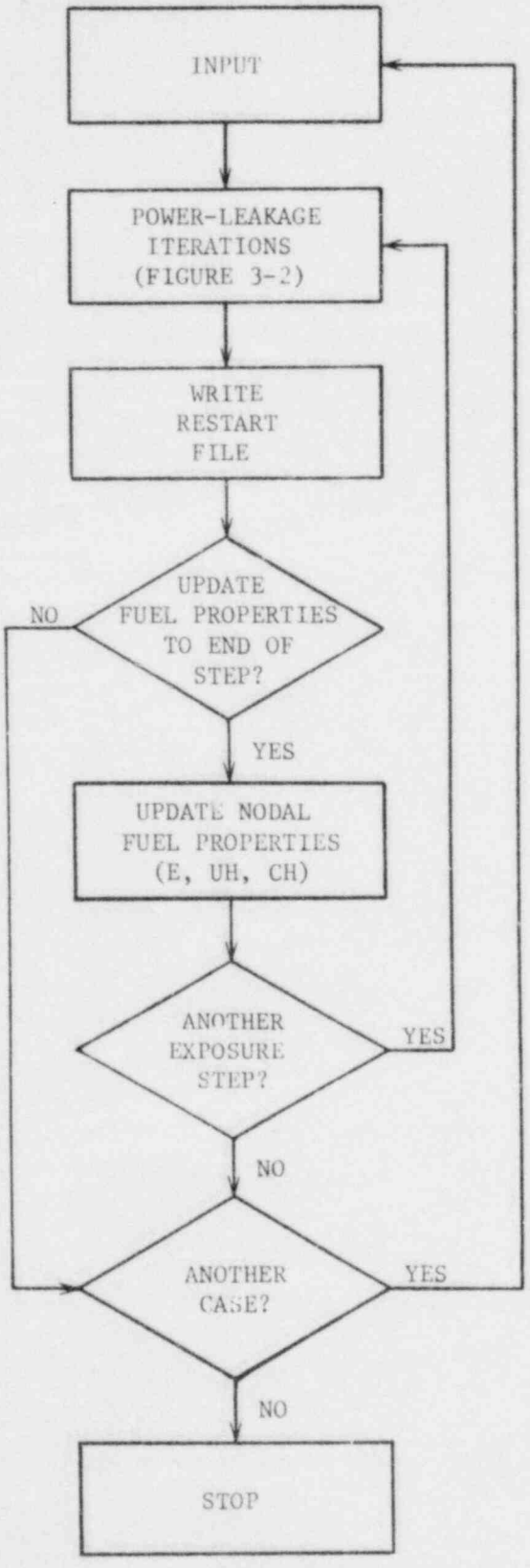

FIGURE 6-1: FORWARD STEP DEPLETION

In this manner, the fuel can be depleted step by step through the cycle.

6.2 POWER-EXPOSURE TECHNIQUE

An alternate procedure for the depletion of a core through a cycle is the Power-Exposure Technique (Reference 6-1). This technique (PET) directly calculates the unique, consistent power and exposure distributions at the end-of-cycle (EOC) given the desired EOC k_{eff}. The method can also be used to step from a known initial state to another exposure level with a specified k_{eff}. The power distribution determined by PET is that of the Haling Principle (Reference 6-2) which, if maintained, gives minimum power peaking throughout the cycle. The Haling distribution is useful for many survey calculations and in the development of target control rod patterns (Section 7.3.3).

The sequence of the PET calculations is shown in Figure 6-2. For an input k_{eff}^{EOC} and a known initial state, the exposure step ΔE and the Haling power distribution $\bar{P}_{ijk}$ are estimated. The EOC or final state nodal fuel properties are updated for iteration n+1:

$$E_{ijk}^{n+1} = E_{ijk}^{BOC} + \bar{P}_{ijk}^{n} \Delta E^{n} \frac{\overline{WT}}{WT_{ijk}} \tag{6-4}$$

$$UH_{ijk}^{n+1} = UH_{ijk}^{BOC} + U_{ijk}^{n} \bar{P}_{ijk}^{n} \Delta E^{n} \frac{\overline{WT}}{WT_{ijk}} \tag{6-5}$$

$$CH_{ijk}^{n+1} = CH_{ijk}^{BOC} + CF_{ijk}^{n} \bar{P}_{ijk}^{n} \Delta E^{n} \frac{\overline{WT}}{WT_{ijk}} \tag{6-6}$$

where the superscript BOC indicates the beginning-of-cycle or initial state values and the other parameters are defined in the previous section. The nodal fuel properties are used in the power-leakage iteration which

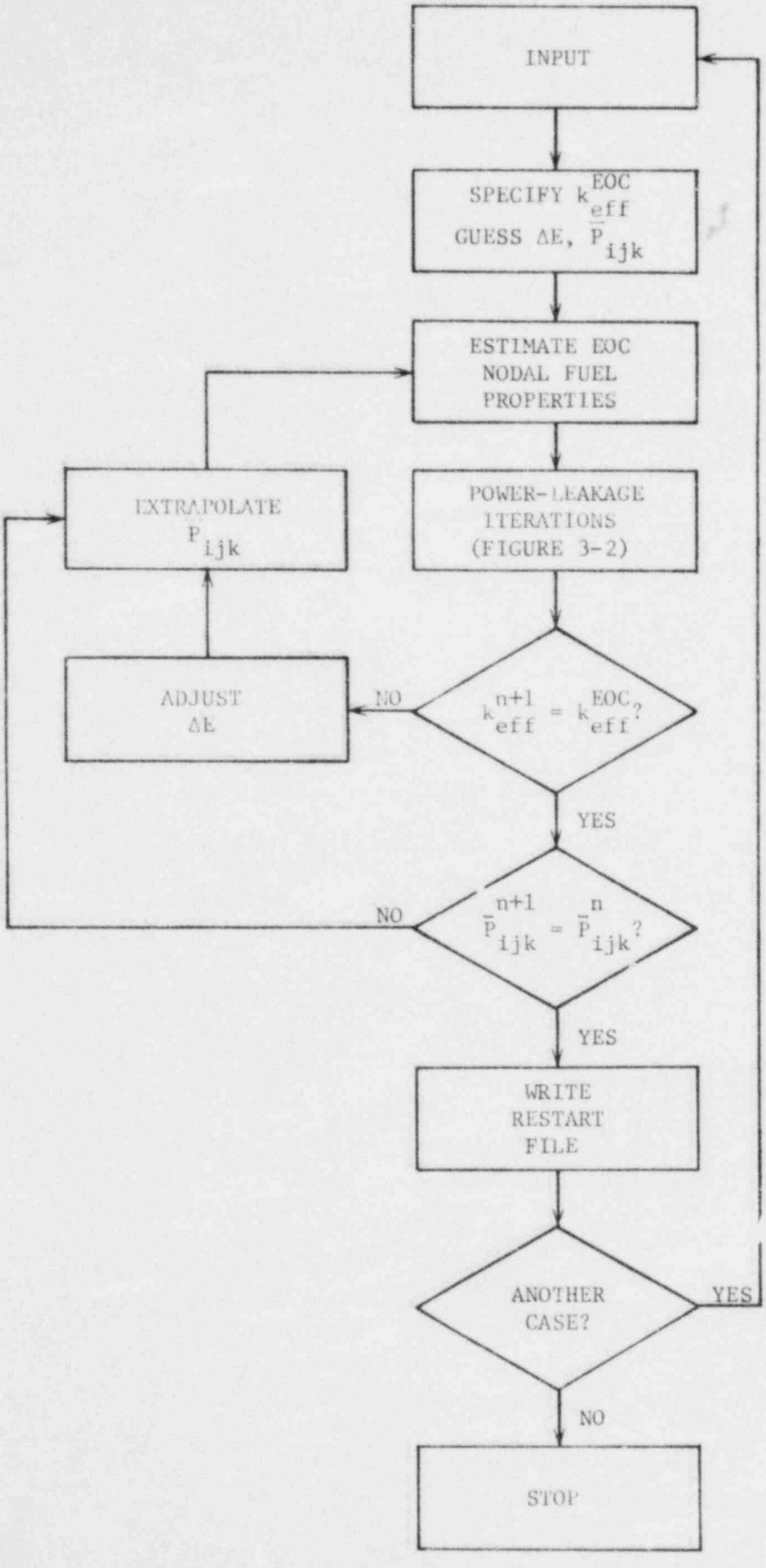

FIGURE 6-2: POWER-EXPOSURE TECHNIQUE

re-estimates k_{eff} and $\bar{P}_{ijk}$. The procedure is repeated with an adjusted ΔE and extrapolated $\bar{P}_{ijk}$ until the power distribution converges and the calculated k_{eff} is equal to the desired value.

CHAPTER 6 REFERENCES

1. R. L. Crowther, "Burnup Analysis of Large Boiling Water Reactors," Proceedings of a Panel on Fuel Burnup Predictions in Thermal Reactors, IAEA, Vienna, 1968.

2. R. K. Haling, "Operating Strategy for Maintaining an Optimum Power Distribution Throughout Life," TID-7672, 1963.

7. AUXILIARY CALCULATIONS

7.1 THERMAL LIMITS

Core thermal performance characteristics can be determined using the converged power distribution (Section 3.5). The thermal limits evaluated consist of peaking factors, linear heat generation rates (LHGR's), and margins with respect to transition boiling. Of course, the core simulator is not intended for monitoring thermal limits, a function of the plant process computer, but for comparison and predictive purposes.

In order to evaluate thermal margin, it is useful to examine the following peaking factors for each node or channel:

a) the nodal local peaking factor F_ℓ is the ratio of the power of the highest powered rod segment in the node to the average rod segment power in that node,

b) the channel peaking factor F_c is the ratio of the power of the channel to the average channel power in the core,

c) the nodal axial peaking factor F_a is the ratio of the power of the node to the average nodal power in its channel,

d) the nodal gross peaking factor $F_g = F_c F_a$ is the ratio of the power of the node to the average nodal power in the core, and

e) the nodal total peaking factor $F_t = F_\ell F_g$ is the ratio of the power of the highest powered rod segment in the node to the average rod segment power in the core.

The local peaking factor is evaluated using input data developed from the detailed lattice physics analysis for each nuclear fuel type. The representation reflects the influence of the configuration of the fuel and control rods around the node as well as the nodal exposure and water density. The

other peaking factors are determined from the relative power distribution. All the peaking factors are edited for the nodal positions corresponding to maximum F_g, maximum F_t, and minimum transition boiling margin.

Utilizing the peaking factors, core thermal power, and assembly design data, the rod segment LHGR and the average planar LHGR can be calculated and compared to limiting values.

LWR's are restricted in operation to conditions that will not lead to the transition from nucleate to film boiling. Two indicators of thermal margin with respect to transition boiling are used: the departure from nucleate boiling ratio (DNBR) for PWR's and the critical power ratio (CPR) for BWR's. Minimum values for these parameters are determined and compared to limiting values in order to evaluate the transition boiling margin.

The DNBR is the ratio of the DNB heat flux to the operating heat flux of the highest powered rod segment in a particular node. The DNB heat flux is that required to cause transition boiling at any location in the node and is calculated as an option using the W-3 correlation (Reference 7-1).

The CPR is the ratio of the channel power required to initiate transition boiling at any location in the channel to the operating channel power. Generally, either the critical heat flux or quality at the point of transition is related to power to create a critical power correlation. The correlations used include CISE (Reference 7-2), XN-2 (Reference 7-3) and an assembly power limit method (Reference 7-4). The CISE formulation uses the critical quality and the XN-2 correlation calculates the critical heat flux for conversion to the critical power. The assembly power limit method is similar to that used in TVA's Browns Ferry Nuclear Plant process computer and in

the auxiliary method described in Reference 7-4. A precalculated base critical power, provided as a function of nuclear fuel type, channel flow and exposure, is adjusted to account for the effects of axial peaking, total core flow rate, and inlet subcooling.

7.2 SIMULATED IN-CORE DETECTOR READINGS

LWR's incorporate fission chamber detectors at fixed radial locations as axially traversing in-core probes (TIP) or fixed monitors to measure operating power distributions. These detectors are located in guide thimbles in the bypass region between fuel assemblies for BWR's and within the assembly itself for PWR's.

7.2.1 Traversing In-Core Probes

Since the detectors are fission chambers, the response at any location is proportional to the fission rate of the detector at that location:

$$R_{\ell k} = C \frac{V}{I} \sum_i \left(\frac{A}{P}\right)_{i\ell k} P_{i\ell k} \qquad (7\text{-}1)$$

where

$R_{\ell k}$ = the TIP reading at radial location ℓ and axial level k,

$P_{i\ell k}$ = the power density in node i adjacent to the detector at position ℓ,k;

$\left(\frac{A}{P}\right)_{i\ell k}$ = the ratio of the fission rate in the detector to the power density of node i, determined from a correlation of detailed lattice physics data as a function of the nodal water density, exposure, and control fraction for each nuclear fuel type,

V = the volume of the detector,

C = a proportionality constant, and

the summation is over the I nodes directly adjacent to the detector. Thus the possible variation in nuclear fuel types around the detector is taken into account.

Simulated TIP readings are made for each real or pseudo detector location (Figure 2-1) at each axial level. Then the readings are normalized to those for a specified detector thimble:

$$R^n_{\ell k} = C_n \frac{R_{\ell k}}{\bar{R}_m} \qquad (7\text{-}2)$$

where

$R^n_{\ell k}$ = the normalized TIP reading at position ℓ,k;

$\bar{R}_m$ = the average reading for the specified detector thimble which is located at the radial position m, and

C_n = the input normalization value of $\bar{R}_m$.

7.2.2 Fixed Monitors

After the normalized TIP readings are calculated, simulated signals for fixed in-core monitors can be generated for BWR's. Local power range monitors (LPRM's) are located at fixed axial levels throughout the core in order to continuously monitor the power distribution. Average power range monitors (APRM's) combine signals from several LPRM's to estimate the total power generated in the core. Rod block monitors (RBM's) are used to restrict control rod withdrawal based on the power change in the region affected by the rod. The required RBM signal is obtained by averaging the signals of the LPRM's adjacent to the control rod. Thus only LPRM signals need to be evaluated.

The LPRM signals are determined using the input detector locations and the calculated TIP readings. If the LPRM is located on an axial level boundary, then its signal is the average of the TIP readings for the nodes

above and below the boundary. Otherwise, the LPRM reading is set equal to the TIP reading at the detector location. The APRM and RBM signals can be calculated as the average of the appropriate LPRM signals.

7.3 SPECIAL FUEL MANAGEMENT FEATURES

7.3.1 Fuel Isotopics

The fissile and fertile fuel isotopic concentrations can be determined if the fuel properties (exposure, water density history, and control history) are available from a previous CORE run or from the plant process computer. Nodal values of E, $\overline{U}$ and $\overline{CF}$ are used to interpolate the isotopics from input table sets described in Section 5.1. The mass of each of the following materials is tabulated on a nodal basis: U-235, U-236, U-238, Pu-239, Pu-240, Pu-241, Pu-242, fissile Pu and total Pu. Summations of nodal values are made to obtain the isotopic content by physical fuel type, by assembly, in specific core regions, or in the entire core.

7.3.2 Relative Control Rod Worths

In order to calculate the core shutdown margin, it is necessary to determine the highest worth control rod. A simple perturbation technique is used to estimate the worth of each control rod relative to the other rods by a weighted change in multiplication factor of the affected nodes when the control rod is withdrawn. The shutdown margin is then determined by performing detailed calculations using the core simulator for several of the rods having the highest relative worth.

7.3.3 Target Control Rod Patterns

Target control rod patterns are used to guide plant operations. As an aid in developing these patterns, CORE contains an algorithm (Reference 7-5) which estimates the rod pattern required to approximate a

specified power distribution, normally the Halin distribution calculated with the power-exposure technique (Section 6.2). This option is valid only for those reactors that use control rods for power shaping, i.e., BWR's. The algorithm is based on the following guidelines:

a) the control rod pattern should minimize the deviation of the k_∞ distribution from that associated with the desired power shape;

b) the control rods are grouped into two basic checkerboard patterns with half the rods in each pattern. Only one pattern can be used at any time. Each pattern is subdivided into diagonally alternating deep and shallow rods;

c) the control rods are withdrawn in a sequence such that the distances between inserted rods and the distances between inserted rods and the core boundary are optimized to reduce interaction between control rods; and

d) all symmetrically located rods are inserted the same distance into the core in order to maintain core symmetry.

The control fraction required in each node ijk to obtain the desired power distribution for a specified core k^d_{eff} is determined from

$$CF_{ijk} = \frac{k^u_{\infty_{ijk}} - \frac{k^d_{eff}}{k^p_{eff}} k^p_{\infty_{ijk}}}{k^u_{\infty_{ijk}} - k^c_{\infty_{ijk}}} \qquad (7\text{-}3)$$

where

k^u_∞ = the nodal multiplication factor with the control rod withdrawn,

k^c_∞ = the nodal k_∞ with the control rod inserted,

k_{∞}^{p} = the nodal k_{∞} associated with the desired power distribution, and

k_{eff}^{p} = the core k_{eff} associated with the power distribution.

The number of control rods at axial level k corresponding to the required control distribution is estimated by

$$N_k = \frac{1}{4} \sum_{i=1}^{I} \sum_{j=1}^{J} CF_{ijk} \qquad (7\text{-}4)$$

where the division by 4 is necessary since each control rod controls four fuel assemblies in a BWR.

Since control rods are inserted from the bottom of the core, the number of rods inserted at level k cannot be larger than at level k-1. The distribution calculated by Equation (7-4) may not satisfy this requirement. Therefore, a pattern search procedure (Reference 7-6) is used to find the monotonically decreasing distribution with the minimum least squared deviation from N_k. The revised distribution is used to establish the number of control rods inserted at each axial level. The individual rod groups to be inserted are selected based on the guidelines presented earlier. Control rod patterns developed by this method can be evaluated by performing a normal simulator calculation.

7.3.4 Fuel Reload Patterns

An algorithm is available to assist in the development of a fuel reload pattern for a cycle. The algorithm uses random assignment and exhaustive enumeration of exchanges in fuel assembly positions to generate trial reload patterns. Quarter core symmetry with both automatic and user-specified shuffling instructions is used to reduce the number of feasible patterns to

be searched. The deviation from a desired power distribution is employed as the objective function which is estimated after each assembly movement based upon the local distribu' on of assembly infinite multiplication factors. The desired distribution is that which yields maximum reactivity within a constraint on power peaking and is obtained from an auxiliary pattern search routine (Reference 7-6).

The user-specified shuffling instructions restrict the possible assignments of the fuel assemblies:

a) discharge specified assemblies,

b) insert fresh assemblies into specified locations,

c) move selected assemblies into specified locations, and

d) restrict the assignment of selected assemblies to within a set of specified locations.

The automatic instructions have lower priority than those specified by the user and, in order of implementation, include

a) discharge the fuel assemblies with the lowest ıctivities to make up the total required number of assemblies to be discharged,

b) randomly insert the required number of fresh fuel assemblies into available locations, and

c) randomly assign assemblies to available locations.

The above instructions are incorporated in an assignment table that controls the movements of the assemblies. The table is dimensioned for a quarter core and indicates the permissible assignments for each ı. l assembly. If the problem is a half or full core case, assemblies with similar fuel properties to those in the modeled quadrant are assigned to symmetric locations in the remaining quadrants.

The number of fuel assemblies to be shuffled simultaneously can be varied from two to the total in the quarter core. Reload patterns are generated until a limit on the number of assembly movements is reached. The pattern with the minimum value of the overall objective function is designated as the best pattern. This optimization technique does not guarantee that a global optimum pattern will be reached. However, a good fuel reload pattern can be obtained through the use of a good initial fuel pattern and a logical set of shuffling instructions. The generated pattern can be refined by the user as necessary and evaluated by a detailed simulator calculation.

7.3.5 Additional Capabilities

The CORE code also has the capability to automatically adjust a specified parameter during the power-leakage iterations to achieve an input value of the effective multiplication factor. Parameters available for adjustment include the total core flow, thermal power, inlet subcooling, and soluble boron concentration.

In order to calculate reactivity coefficients and adiabatic reactivity worths, various thermal-hydraulic properties can be held constant at values from a previous case while performing the power-leakage iterations. The combinations of parameters include

a) the water density, moderator temperature, and effective fuel temperature,

b) the water density and moderator temperature, or

c) the effective fuel temperature.

The nodal xenon concentration can also be held constant with any of the above combinations.

CHAPTER 7 REFERENCES

1. L. S. Tong, "Prediction of Departure from Nucleate Boiling for an Axially Non-Uniform Heat Flux Distribution," J. Nucl. Energy, Vol. 21, pp. 241-248, 1967.

2. L. S. Tong, "Boiling Crisis and Critical Heat Flux," TID-25887, 1972.

3. K. Galbraith and J. Jaech, "The XN-2 Critical Power Correlation," XN-75-34-A, 1975.

4. V. W. Mills, "TBAR Method for LPRM Calibration and Core Performance Evaluation for Browns Ferry Unit 3 Cycle 1," NEDC-21366, 1976.

5. T. L. Hayslett, Jr., "MYROD, A Computer Program for Predicting Control Rod Patterns for a Boiling Water Reactor," Master's Thesis, Department of Nuclear Engineering, Mississippi State University, 1976.

6. R. Hooke and T. A. Jeeves, "Direct Search Solution of Numerical and Statistical Problems," J. Assoc. for Computing Mach., Vol. 8, pp. 219-229 1961.

APPENDIX

THAS THERMAL-HYDRAULICS CODE

The THAS code developed by TVA performs the thermal-hydraulic analysis of a single heated channel for the range of operating conditions in LWR cores. The equations of conservation of energy and momentum are applied to control volumes defined by dividing the channel into a number of equal length segments. Nonboiling, subcooled boiling and bulk boiling conditions are treated. Experimentally based correlations are used to calculate the flow quality, the steam void fraction, the distributed friction loss coefficient, and local pressure losses. Water and steam properties are determined from the 1967 ASME formulas (Reference A-1) except for a least squares fit of the surface tension.

A.1 COOLANT ENTHALPY DISTRIBUTION

Conservation of energy in each control volume implies

$$H_{out} = H_{in} + C \frac{FP_c}{W} \qquad \text{(A-1)}$$

where

H_{out} = the coolant enthalpy at the volume outlet,

H_{in} = the coolant enthalpy at the volume inlet,

W = the mass flow rate through the channel,

P_c = the channel power,

F = the fraction of power in the control volume, and

C = a conversion factor.

The above equation is valid for all flow regimes.

A.2 VOID FRACTION AND QUALITY

The fraction of steam voids in the coolant is calculated from

$$\alpha = \frac{\chi}{\chi + \frac{\rho_g}{\rho_f} S(1-\chi)} \qquad \text{(A-2)}$$

where

χ = the flow quality,

S = the slip ratio evaluated using the CISE model discussed in Section 4.3.3,

ρ_g = the density of saturated steam, and

ρ_f = the density of saturated water.

Flow quality is defined as the ratio of the flow rate of steam to the total flow rate in the channel:

$$\chi = \frac{W_g}{W} \qquad \text{(A-3)}$$

The flow quality in the bulk boiling regime is equal to the thermodynamic quality χ_e

$$\chi = \chi_e = \frac{H - H_f}{H_g - H_f} \qquad \text{(A-4)}$$

where

H = the local coolant enthalpy,

H_f = the enthalpy of saturated water, and

H_g = the enthalpy of saturated steam.

In subcooled boiling, thermodynamic equilibrium does not exist and the flow quality is calculated from the Levy correlation (Reference A-2).

Levy's method begins by finding the subcooling at bubble detachment $\Delta T_d = T_s - T_b$ as a function of a dimensionless distance Y_B characteristic

of the bubble layer thickness:

$$\Delta T_d = \begin{cases} \Delta T_{sp} - Q Pr_\ell Y_B & 0 \le Y_B \le 5 \\ \Delta T_{sp} - 5Q \left\{ Pr_\ell + \ln \left[1 + Pr_\ell \left(\frac{Y_B}{5} - 1 \right) \right] \right\} & 5 \le Y_B \le 30 \\ \Delta T_{sp} - 5Q \left[Pr_\ell + \ln(1 + 5Pr_\ell) + \frac{1}{2} \ln \left(\frac{Y_B}{30} \right) \right] & Y_B \ge 30 \end{cases} \quad \text{(A-5)}$$

The dimensionless distance Y_B is derived from a force balance on a bubble:

$$Y_B = \frac{0.015}{\mu_\ell} \sqrt{\sigma g_c D_e \rho_\ell} \quad \text{(A-6)}$$

where

μ_ℓ = the viscosity of water,

ρ_ℓ = the density of water,

σ = the surface tension of the bubble, and

D_e = the equivalent diameter of the channel.

The single phase subcooling ΔT_{sp} is given by

$$\Delta T_{sp} = \frac{q''}{h_{sp}} \quad \text{(A-7)}$$

where q" is the heat flux out of the surface and h_{sp} is the single phase heat transfer coefficient calculated from the Dittus-Boelter correlation

$$h_{sp} = 0.023 \frac{k_\ell}{D_e} Re_\ell^{0.8} Pr_\ell^{0.4} \quad \text{(A-8)}$$

The thermal conductivity of water is denoted by k_ℓ; Re_ℓ and Pr_ℓ are the Reynolds and Prandtl numbers, respectively, evaluated at the bulk liquid temperature. The parameter Q in Equation (A-5) is defined as

$$Q = \frac{q''}{C_p \sqrt{\tau_w g_c \rho_\ell}} \quad \text{(A-9)}$$

where C_p is the specific heat of water. The wall shear stress is

$$\tau_w = f \frac{G^2}{8 g_c \rho_\ell} \tag{A-10}$$

where G is the mass flux through the control volume and f is the Darcy-Weisbach friction factor

$$f = aRe^b + c \tag{A-11}$$

with the constants a, b, and c supplied by the user.

Then the quality at bubble detachment is calculated

$$\chi_d = - \frac{C_p \Delta T_d}{H_{fg}} \tag{A-12}$$

and the subcooled flow quality is interpolated by

$$\chi = \begin{cases} 0 & \chi_e \leq \chi_d \\ \chi_e - \chi_d \exp\left(\frac{\chi_e}{\chi_d} - 1 \right) & \chi_e \geq \chi_d \end{cases} \tag{A-13}$$

A.3 FLOW AND PRESSURE DROP

Conservation of momentum in the control volume is expressed as a pressure loss between the inlet and outlet to the volume. The total pressure drop across a control volume is the sum of components from friction, elevation, acceleration, and local effects:

$$\Delta P = \Delta P_f + \Delta P_h + \Delta P_a + \Delta P_s \tag{A-14}$$

At the user's option, the flow can be fixed to determine the pressure drop, or can be changed iteratively until the channel pressure drop reaches a preset value.

The friction pressure drop is calculated from the Darcy-Weisbach equation

$$\Delta P_f = f \phi_f \frac{\Delta Z}{D_e} \frac{G^2}{2 g_c \rho_\ell} \tag{A-15}$$

where

f = the Darcy-Weisbach single phase friction factor,

ϕ_f = the two-phase multipler of the friction factor, and

ΔZ = the length of the control volume.

The two-phase friction multiplier is interpolated as a function of mass flux and quality in tables developed from Baroczy's correlation (Reference A-3).

The elevation pressure drop is calculated from

$$\Delta P_h = \left[\alpha\rho_g + (1-\alpha)\rho_\ell\right] \Delta Z \frac{g}{g_c} \tag{A-16}$$

where g is the acceleration of gravity.

The pressure loss due to acceleration of the coolant as it is heated is

$$\Delta P_a = \frac{1}{g_c}\left[\alpha\rho_g v_g^2 + (1-\alpha)\rho_\ell v_\ell^2\right]_{out} - \frac{1}{g_c}\left[\alpha\rho_g v_g^2 + (1-\alpha)\rho_\ell v_\ell^2\right]_{in} \tag{A-17}$$

where

v_g = the velocity of the vapor phase

$= \frac{\chi}{\alpha} G$

v_ℓ = the velocity of the liquid phase

$= \frac{(1-\chi)}{(1-\alpha)} G$

The local pressure losses are caused by changes in flow area along the channel, such as spacers:

$$\Delta P_i = K\phi_\ell^i \frac{G^2}{2g_c\rho_\ell} \tag{A-18}$$

The single phase local loss coefficient K is an input parameter, and the two phase local loss multiplier ϕ_ℓ^i used is a modified Romie multiplier (Reference A-4):

$$\phi_\ell^i = \frac{(1-\chi)^2}{(1-\alpha_\infty)} + \frac{\chi^2}{\alpha_\infty}\frac{\rho_f}{\rho_g} \qquad \text{(A-19)}$$

where

$$\alpha_\infty = \frac{\alpha_h}{C_i + \alpha_h(1-C_i)} \qquad \text{(A-20)}$$

The parameter α_h is the void fraction assuming homogeneous flow, and C_i is an empirical constant which depends on the flow restriction. Note that this pressure drop is omitted for control volumes in which no spacer is located.

The inlet pressure to the first control volume is determined by subtracting the inlet pressure loss from the input lower plenum pressure. Then the above calculations are performed successively for each control volume using the outlet conditions of the lower volume as the inlet conditions for the next. The channel outlet pressure is obtained by subtracting the exit pressure loss from the outlet pressure of the uppermost control volume.

APPENDIX REFERENCES

1. C. A. Meyer, et al., "Thermodynamic and Transport Properties of Steam," American Society of Mechanical Engineers, 1967.

2. S. Levy, "Forced Convection Subcooled Boiling - Prediction of Vapor Volumetric Fraction," GEAP-5157, 1966.

3. C. J. Baroczy, "A Systematic Correlation for Two-Phase Pressure Drop," Chem. Eng. Prog. Symp. Ser. No. 64, Vol. 62, 1964.

4. J. A. Wooley, "Three-Dimensional BWR Core Simulator," NEDO-20953A, 1977.